A Low Latitude Halo Stream around the Milky Way

Brian Yanny[1,2], Heidi Jo Newberg[1,3], Eva K. Grebel[4], Steve Kent[2] Michael Odenkirchen[4], Connie M. Rockosi[5], David Schlegel[6], Mark Subbarao[7], Jon Brinkmann[8], Masataka Fukugita[9], Željko Ivezic[6], Don Q. Lamb[7], Donald P. Schneider[10], Donald G. York[7]

ABSTRACT

We present evidence for a ring of stars in the plane of the Milky Way, extending at least from $l = 180°$ to $l = 227°$ with turnoff magnitude $g \sim 19.5$; the ring could encircle the Galaxy. We infer that the low Galactic latitude structure is at a fairly constant distance of $R = 18 \pm 2$ kpc from the Galactic Center above the Galactic plane, and has $R = 20 \pm 2$ kpc in the region sampled below the Galactic plane. The evidence includes five hundred SDSS spectroscopic radial velocities of stars within 30° of the plane. The velocity dispersion of the stars associated with this structure is found to be 27 km s^{-1} at $(l, b) = (198°, -27°)$, 22 km s^{-1} at $(l, b) = (225°, 28°)$, 30 km s^{-1} at $(l, b) = (188°, 24°)$, and 30 km s^{-1} at $(l, b) = (182°, 27°)$. The structure rotates in the same prograde direction as the Galactic disk stars, but with a circular velocity of 110 ± 25 km s^{-1}. The narrow measured velocity dispersion is inconsistent with power law spheroid or thick disk populations. We compare the velocity dispersion in this structure with the velocity dispersion of stars in the Sagittarius dwarf galaxy tidal stream, for which we

[1]Equal first authors

[2]Fermi National Accelerator Laboratory, P.O. Box 500, Batavia, IL 60510; yanny@fnal.gov; skent@fnal.gov

[3]Dept. of Physics, Applied Physics and Astronomy, Rensselaer Polytechnic Institute Troy, NY 12180; heidi@rpi.edu

[4]Max Planck Institute for Astronomy, KonigStuhl 17, D-69117 Heidelberg, Germany

[5]University of Washington, Seattle, Washington

[6]Princeton University, Princeton NJ 08544

[7]Dept. of Astronomy and Astrophysics, University of Chicago, 5640 S. Ellis Ave., Chicago, IL 60637

[8]Apache Point Observatory, P. O. Box 59, Sunspot, NM 88349-0059

[9]University of Tokyo, Institute for Cosmic Ray Research, Tokyo, Japan

[10]Department of Astronomy and Astrophysics, The Pennsylvania State University, University Park, PA 16802

measure a velocity dispersion of 20 km s^{-1} at $(l, b) = (165°, -55°)$. We estimate a preliminary metallicity from the Ca II (K) line and color of the turnoff stars of $[Fe/H] = -1.6$ with a dispersion of 0.3 dex and note that the turnoff color is consistent with that of the spheroid population. We interpret our measurements as evidence for a tidally disrupted satellite of 2×10^7 to $5 \times 10^8 M_\odot$ which rings the Galaxy.

Subject headings: Galaxy: structure — Galaxy: halo

1. Introduction

The Milky Way Galaxy's system of stars is generally divided into several global components based on broad positional, kinematic and chemical abundance information. Major components are: thin disk, thick disk, spheroidal halo, and bulge. There is recent evidence, however, that these basic components do not explain all of the stars seen in photometric and spectroscopic surveys.

Larsen & Humphreys (1996) and Parker, Humphreys, & Larsen (2001) report a significant asymmetry in the number of stars in the thick disk/inner halo from one side of the Galactic Center to the other, at angles of $20° - 75°$ from a Galactic longitude of zero, at $20° < b < 50°$. The stars are approximately 3 kpc from the Sun. They suggest this asymmetry could indicate triaxial distributions of thick disk or inner halo stars, or could result from interactions of the disk with the Sagittarius dwarf or the Milky Way's bar.

Figure 3 of Alard (2001) shows a 35% asymmetry between the number of stars 6 degrees above and below the plane, at $l = 240°$. They do not quote a typical distance to their stars, but since this study uses brighter 2MASS stars, they must be within a few kiloparsecs of the Sun.

There are several groups who see evidence of a disk-like distribution of metal-weak ([Fe/H] ~ -1.6) stars, which extends to larger scale heights and lower metallicities than the canonical thick disk of Gilmore & Wyse (1985). Norris, Bessell, & Pickles (1985) found a set of stars with orbits like disk stars and metallicities like halo stars, and interpreted these as a metal-weak tail to the thick disk population. Morrison, Flynn, & Freeman (1990) confirmed and extended this result, and Majewski (1993) measured a vertical scale height of the metal-weak thick disk of 2 kpc (twice the canonical scale height of the stars of typical metallicity in the thick disk component).

It is not known whether the Galactic disk is formed from separate disk components, or

whether there is a single disk component with a metallicity and age gradient. In particular, there is no consensus on whether the metal-weak thick disk is part of the proposed Galactic thick disk, or whether it is itself a separate component (Beers et al. 2002).

Gilmore, Wyse, & Norris (2002) find a group of stars, within 3-5 kpc of the Sun at $l \sim 270°$, which is rotating more slowly about the Galactic center than would be expected of a thick disk population. The stars are found 30° above and 45° below the Galactic plane (5 kpc apart). They interpret these stars as originating in a satellite galaxy which merged with the Milky Way and perhaps could have created the thick disk.

There are other indications that smooth galaxy components of star distributions in the Milky Way do not yield the complete picture. Moving groups and halo substructure have been observed from stellar kinematics (Helmi et al. 1999; Majewski, Munn, and Hawley 1996). Tidal disruption of globular clusters and the Sagittarius dwarf galaxy in the halo of our Milky Way galaxy have been documented (Odenkirchen et al. 2001; Mateo, Olszewski & Morrison 1998; Majewski et al. 1999; Martinez-Delgado et al. 2001; Vivas et al. 2001; Rockosi et al. 2002; Kundu et al. 2002; Bellazzini, Ferraro, & Ibata 2002) in spatial star-density and kinematic studies.

Deep, accurate, multi-color Sloan Digital Sky Survey (SDSS, see York et al. 2000) photometry of blue stars was used by Yanny, Newberg et al. (2000) and Newberg, Yanny et al. (2002), hereafter designated Paper I and Paper II, to probe the structure of the Milky Way's halo over a distance range $2 < d < 150$ kpc. Paper I identified large structures (length scales > 10 kpc) of stars which turned out to be two pieces of the tidal stream of the Sagittarius dwarf galaxy (Ibata et al. 2001a). Paper II showed the Sagittarius dwarf stream turnoff stars and color-magnitude diagrams (CMDs), and also identified additional substructure in the Galactic halo. The most striking discovery was the identification of a large number of blue stars at low Galactic latitudes, roughly in the direction of the Galactic anti-center.

Each overdensity of stars identified in Paper II was designated with a label of the form S$l \pm b - g$, where $(l \pm b)$ are the approximate center in Galactic coordinates and g is the approximate g magnitude of the F dwarf stars in that overdensity. Since many of the structures we are looking at cover large areas of the sky (for example the stream of the Sagittarius dwarf galaxy), it is likely as we obtain additional SDSS imaging data that the many identified overdensities will eventually connect to trace large structures. We concluded in Paper II that the overdensities S223+20-19.4, S218+22-19.5, S183+22-19.4, and (with less significance) S200-24-19.8 were parts of the same large structure in the sky, since they had similar CMDs, turnoff colors, and inferred distances. The sky positions of these overdensities are spread over 40° of Galactic latitude and 40° of Galactic longitude.

In Paper II we explored two possible explanations for the unexpectedly high concentrations of stars near the Galactic anti-center: either the stars are part of the tidal stream from a tidally disrupted dwarf galaxy, or they are part of the "metal-weak thick disk" described above.

One of these structures, at $(l, b) = (198°, -27°)$, was selected for spectroscopic followup, and we present here radial velocities of several hundred faint $g \sim 20$ blue stars in that structure. In addition, we present serendipitous SDSS spectra of $18.5 < g < 19.5$ stars in several other directions of interest and make a case that stars in three of these directions are pieces of the same low-latitude stream, at a distance of 18 kpc from the Galactic center. We also consider the possibility that the stars are part of a shell such as that seen around some elliptical galaxies which have undergone mergers (Malin & Carter 1983; Merrifield & Kuijken 1998; Tremaine 1999).

The case for the existence of a stream ringing the Galaxy is made in this paper as follows: The instrumentation and observing system of the SDSS is reviewed in §2, and the accuracy with which radial velocities obtained with the SDSS are known relatively and absolutely is justified in §4. In §3 and §6, radial velocities of a set of faint blue turnoff stars, defined to be stars of spectral type F with absolute magnitudes of about $M_g = 4.2 \pm 0.3$, are observed at several positions around the sky. At low Galactic latitudes, these stars at implied distances of 17-20 kpc from the Galactic center are shown to have a remarkably narrow velocity dispersion, inconsistent with a stellar spheroidal halo population. Combined with the narrow appearance of the stars' faint turnoff in the photometric color-magnitude diagram, we argue that the distribution is annular in nature. A comparison to a known stream is discussed in §5. Using the observed velocities and positions of stars over an arc of 50° on the sky we constrain the possible orbits of stars in this coherent structure in §7 and discuss further details in §8. Finally, we summarize in §9.

After submission of this paper, Ibata et al. (2003) circulated a paper showing that the stream extends to the vicinity of the Andromeda galaxy, extending the known extent of the structure from 50° to 100° of arc on the sky, as seen from the Sun.

2. SDSS Technical Details

A main goal of the SDSS is to obtain the redshifts of nearly one million galaxies and one hundred thousand quasars. These are obtained with 45 minute long exposures with a 640 fiber double spectrograph on the SDSS 2.5m telescope (York et al. 2000). The targets are selected from SDSS imaging data, and holes at the positions of bright galaxies, stars

and other targets of interest are drilled in 1 m diameter aluminum plates, which cover a 3° diameter field of view.

During normal SDSS operations, stellar objects are targeted in about 35 to 80 of the 640 fibers on any given plate. Sixteen of these targets on each plate are moderately bright objects, called SDSS reddening and spectrophotometric stars, and are used to calibrate all the objects on a given plate. They are generally F subdwarfs with $16 < g < 18.5$. There are also 10-30 fibers placed on objects of interesting color, generally blue or red objects off the usual stellar locus, including blue horizontal branch stars, brown subdwarfs, and white dwarfs. In addition, about 35% of fibers placed on quasar candidates turn out to be stars in the Galaxy rather than actual quasars. In this way, a large sample of stellar spectra are obtained with signal-to-noise greater than 10 to limits of $g \sim 20.0$ over the course of the survey.

Here and throughout the paper, SDSS magnitudes and filters are designated without superscripts: u, g, r, i, z. This indicates that the magnitudes are on the 2.5m imaging camera system, which is closely tied to the SDSS photometric system. See Smith et al. (2002); Fukugita et al. (1996); Hogg et al. (2001) for details on the SDSS photometric system and the SDSS photometric monitor. See Gunn et al. (1998); Lupton et al. (2003) for details on the SDSS imaging camera system and imaging processing software. A subscript '0' on a magnitude or color indicates that it has been corrected by applying the full dereddening appropriate for its position on the sky. We correct these magnitudes for reddening using $E(B-V)$ from Schlegel, Finkbeiner, & Davis (1998), which has spatial resolution of 0.1 degrees, and the standard extinction curve, which for SDSS filters yields: $A_{u^*} = 5.2E(B-V); A_{g^*} = 3.8E(B-V); A_{r^*} = 2.8E(B-V)$. The astrometry of SDSS objects is good to better than 100 mas and techniques used in obtaining this accuracy are described in Pier et al. (2002).

During standard SDSS spectroscopic observing, each plate is exposed for 3×15 minutes $= 45$ minutes on the 2.5m SDSS telescope (York et al. 2000) at Apache Point Observatory. Arc lamps of HgHeNeAr are obtained before and after each exposure. Quartz flat exposures of the fibers are also obtained.

The data are processed through the standard SDSS spectroscopic pipelines (software versions v4_9_8 for 2D and v5_7_3 for 1D processing were used), and result in a set of 1D spectra as well as a radial velocity for each object based on cross correlations against a high signal-to-noise (S/N) template F star. Additionally, the observed wavelengths and equivalent widths of common lines like Ca II K and the Balmer lines are measured. The line positions give a second measure of radial velocity in addition to the template match, and the agreement between the two does not conflict with our estimated radial velocity errors for fainter stars

of $\sigma = 16 - 20\,\mathrm{km\,s^{-1}}$, which are derived in §4.

The exact selection function of SDSS regular program stellar spectra is complex, but the corresponding imaging data are complete several magnitudes beyond the spectroscopic sample magnitude limit. Thus, color and number count information from the imaging can be used to estimate completeness of any spectroscopic sample. The algorithm by which a mosaic of 3° diameter spectroscopic tiles are selected on the sky is described in Blanton et al. (2002).

3. F star plate 797

We took advantage of an opportunity when none of the normal SDSS program areas were visible to use the fibers in one specially designed spectroscopic plate to study the dynamics of the stars identified in Paper II as belonging to the overdensity S200-24-19.8. The name indicates the stars are near $(l, b) = (200°, -24°)$ and the turnoff is at approximately $g_0 = 19.8$. With an estimated absolute magnitude of $M_g = 4.2$ for these blue stars, this puts the overdensity at a distance of 13.2 kpc from the Sun.

Figure 1 shows a portion of Figure 15 from Paper II, which contains SDSS photometry in a $(g-r)_0, g_0$ color magnitude diagram of stars near $(l, b) = (198°, -27°)$. Note the faint turnoff at $(g-r)_0 = 0.2$, $g_0 = 19.5$. This turnoff has many more stars than the thin or thick disk populations at the same implied distance from the Sun along this Galactic sight-line.

Unlike the usual SDSS science plates, which target about 500 galaxies, 100 QSO candidates and 30 stars per plate, this special plate 797 was arranged to target about 600 blue stellar objects with $19.1 < g_0 < 20.3$ and $0.16 < (g-r)_0 < 0.3$. A handful of objects outside of this range, including eight spectrophotometric and eight reddening stars at $g_0 \sim 17$ and $g_0 \sim 18.25$ respectively, and a few objects with $(g-r)_0 > 0.4$, were also targeted for quality control. The area in color-magnitude space where the spectroscopic targets on plate 797 were selected is indicated by the triangular points in Figure 1.

Plate 797 was exposed for a total of 7200 s on the nights of 2001 December 19 and 20 with the SDSS spectrographs, and processed with standard SDSS software for spectroscopic reductions. This produced a set of fully extracted, wavelength and flux calibrated 1D spectra.

Each of the $\sim$ 600 F-star spectra was examined individually. Since no $(u-g)_0$ color cut was applied to the selection of objects on this particular plate, spectra of numerous hot objects, unrelated to the target F turnoff stars, were observed. Spectra of about 50 quasars and numerous white dwarfs, as well as spectra with S/N too low to measure an accurate

radial velocity, were rejected. Rejecting objects with S/N less than about 5:1 effectively sets our faint limit for obtaining a good radial velocity on this plate at about $g = 20.5$. This left 392 good F star spectra, including the brighter reference F and G stars at $17.0 < g_0 < 18.5$.

A sampling of the good plate spectra shows that the typical S/N for these spectra ranged from about 10 at $g_0 = 19.5$ to about 5 at $g_0 = 20.1$. Individual positions, magnitudes, colors, SDSS IDs, radial velocities, and the equivalent width of the Ca II K λ3933 Å line (W_K) for each good spectrum are listed in Table 1 (full table is ascii text). Table 1 lists for each object: right ascension, declination (J2000), SDSS imaging identifying code (format run-rerun-camcol-field-id), spectroscopic identifying (format plate-mjd-fiberid), g_0 magnitude, $(g-r)_0$ color and $(u-g)_0$ color, the heliocentric radial velocity in km s^{-1}, W_K, a color cut flag, where a 1 indicates the object is one of 327 in the color magnitude box: ($0.158 < (g-r)_0 < 0.3, 19.1 < g_0 < 20.3$), and the $E(B-V)$ from Schlegel, Finkbeiner, & Davis (1998) used to deredden each object. Figure 2 shows the histogram of observed radial velocities for these 327 stars in the color-magnitude box of plate 797.

One can compare the radial velocity histogram of the stars in Figure 2 with our expectations for the radial velocity distribution of standard Galactic components. Each component (power law spheroid, thick disk, and thin disk) is assigned a nominal Galactic rotation velocity in the solar neighborhood and a velocity dispersion ellipsoid. For each component, we calculate the radial velocity, velocity dispersion, and density of stars at the position and distance of the stars in Figure 2. For the thin disk, we adopt

$$< v_{rot}, \sigma_U : \sigma_V : \sigma_W >=< 220,\ 38 : 25 : 20 >,$$

in units of km s^{-1}; for the thick disk,

$$< v_{rot}, \sigma_U : \sigma_V : \sigma_W >=< 170,\ 60 : 45 : 40 >;$$

and for the halo,

$$< v_{rot}, \sigma_U : \sigma_V : \sigma_W >=< 0,\ 130 : 100 : 85 >,$$

in the same units. These parameters are taken primarily from the compilation in Allen (2000), p. 479. However, we adopted a non-rotating halo component and set the rotation velocity of the thin disk to the rotation velocity of the stars in the solar neighborhood. The results of fitting this model to the data are not sensitive to small differences in our adopted parameters.

The Galactic models are calculated as follows: Since the Galaxy has an essentially flat rotation curve exterior to the solar position out to some large distance, the rotation speed of each component in the solar neighborhood is used as the estimate of the rotation curve at the position of the stars in plate 797 ($d_\odot = 13$ kpc, $r_{GC} = 20$ kpc). First, we convert position

in the Galaxy (l, b, r) to standard Galactic Cartesian coordinates (X, Y, Z). From the X and Y positions, we calculate the components of the rotation velocity in the $(\hat{x}, \hat{y})$ directions:

$$\theta = \tan^{-1} Y/X,$$

$$v_x = v_{rot} \sin\theta,$$

$$v_y = -v_{rot} \cos\theta.$$

The position and velocity of the Sun are taken as: $(X, Y, Z) = (-8, 0, 0)$, $(v_x, v_y, v_z) = (10, 225, 7)$ where distances are in kpc and velocities are in km s^{-1}. If $\hat{r}$ is the unit vector in the direction from the Sun to the portion of the Galaxy which we are studying, then the radial velocity we expect to observe from this component is:

$$v_R = (\vec{V} - \vec{V_\odot}) \cdot \hat{r}.$$

From the previous equation, we deduce that the velocity dispersion in the direction $(\hat{r})$ is given by:

$$\sigma_{rv} = \sqrt{(\hat{x} \cdot \hat{r})^2 {\sigma_x}^2 + (\hat{y} \cdot \hat{r})^2 {\sigma_y}^2 + (\hat{z} \cdot \hat{r})^2 {\sigma_z}^2}.$$

It is in principle very difficult to calculate either the fraction of the stars which should belong to each component of the Galaxy or to additionally calculate an overall normalization. This is because one requires not only all of the parameters in the density model for each component, but also the component normalization (usually in the solar neighborhood) of the star counts, and these must be *for the colors of the stars used to select the spectroscopic sample.* If there are color gradients in any component, then these must be modeled as well. Since we use a blue color cut here, in fact bluer than most of the stars in the thick disk component, we assume the normalization between the thick disk and halo might not be the same as if we had used a redder cutoff. In spite of this known difficulty, we estimate the number of stars expected from each component using the following method.

We adopt a model for the density distribution of each Galactic component which is similar to those used in Figure 20 of Paper II. That Figure plots number counts of observed stars around the celestial equator against models of the number counts expected from standard thin disk, thick disk and halo models. The exponential thin disk has scale height 0.25 kpc and scale length 2.5 kpc. For the (exponential) thick disk, we use a scale height of 1.0 kpc, a scale length of 3 kpc, and a normalization of one in 30 of the thin disk star counts in the solar neighborhood (but see Chen et al. 2001).

We use a spherical, power law halo distribution with $\alpha = -3.5$ and a normalization of one in 500 of the thin disk star counts in the solar neighborhood (Bahcall & Soneira 1984).

We fixed the overall normalization of the model to match Fig. 20 of Paper II; the star counts in the magnitude range $16.5 < g_0 < 17.5$ (with assumed absolute magnitude $M_g = 5.0$, since these stars were selected from a redder population than the stream selection) in the direction $(\alpha_{2000}, \delta_{2000}) = (240^\circ, 0^\circ)$ were fixed to match our measured 388 per square degree. Note that the stars in Fig. 20 of Paper II are selected with $0.2 < (g-r)_0 < 0.5$; normalizations used in this model will produce the number of stars expected per square degree, in the color range $0.2 < (g-r)_0 < 0.5$, in a given distance range (calculated from an apparent magnitude range and estimated absolute magnitude for the typical star in the sample). For reference, $(g-r) = 0.98(B-V) - 0.19$ (Smith et al. 2002). The normalization of the the Galactic components is determined by assuming an absolute magnitude of $M_g = 4.3$ (rather than 4.2 for the plate 797 stars), since the average spectrum is from a star slightly redder than the turnoff stars. The model integrates the star counts expected over the magnitude range $18.9 < g < 20$, which is the selection box for the spectra.

These models predict that there are 5 thick disk stars and 131 halo stars per square degree with $0.2 < (g-r)_0 < 0.5$ in the direction and magnitude ranges of the stars in plate 797. Since these models predict that there should be a factor of 10^5 fewer thin disk stars than thick disk stars, we will assume that there are no thin disk stars in our faint blue sample.

We now estimate the number of blue stars ($0.18 < g-r < 0.28$) we expect to find in the same volume. Figure 15 of Paper II shows a Galactic color magnitude diagram in a direction of sky including that towards plate 797; it is a full version of the color magnitude diagram shown in Figure 1. From Figure 15 of Paper II, we estimate that the slope of the thick disk main sequence is 6.6 in the g_0 vs. $(g-r)_0$ diagram. From that same diagram, we attempt to select a sample of mainly thick disk stars that are all at the same distance (and thus in the same volume). From the SDSS stars in the area of the sky described by $-1.25^\circ < \delta_{2000} < 1.25^\circ$, $70.5^\circ < \alpha_{2000} < 73.5^\circ$, we select the stars with $g_0 > 6.6(g-r)_0 + 15.06$ and $g_0 < 6.6(g-r)_0 + 15.36$. These latter cuts have the effect of selecting stars with $17.7 < g_0 < 18$ at $(g-r)_0 = 0.4$. Of these stars, 97 are in the color range $0.18 < (g-r)_0 < 0.28$ and 664 are in the color range $0.2 < (g-r)_0 < 0.5$. From this, we estimate that there are (very roughly) 15% as many blue stars in the thick disk as there are redder stars at the same distance.

We use the same logic to select a set of primarily halo stars, as judged from Figure 8 of Paper II. We choose stars from the area of sky: $-1.25^\circ < \delta_{2000} < 1.25^\circ$ and $240^\circ < \alpha_{2000} < 243^\circ$. Using the same slope for the main sequence, but shifting the magnitude range so that $20.5 < g_0 < 20.8$ at $(g-r)_0 = 0.4$, we find 270 stars in the color range $0.18 < (g-r)_0 < 0.28$ and 1420 stars in the color range $0.2 < (g-r)_0 < 0.5$. From this we estimate that there are roughly 19% as many blue stars in the halo population as there are redder stars at the same

distance.

The predicted contributions to the radial velocity distribution from the thin disk, thick disk, and power law spheroid components are shown in Figure 2 in red, green, and blue, respectively. The mean and standard deviation of the model Gaussian distribution are derived from the models of each stellar component, and the normalizations are estimates derived from the models and our measurements of stellar distributions in the Galaxy, as described above. The sum of all distributions is shown by a heavy, black, dashed line. These known components only account for 157 of the 325 stars shown in the Figure.

We now estimate the mean and dispersion of the "extra" stars. Since the only components which contribute a significant number of stars to the diagram are the power-law spheroid and the additional population whose properties we wish to measure, we used a maximum likelihood fit to the data in which the model included only two Gaussian distributions. The mean, sigma, and fraction of the observed stars in the extra component were allowed to vary so that the reduced chi-square fit between the model and the data was minimized (reduced chi-squared = 1.33). We fixed the total number of stars as the observed number of stars, but allowed the relative amplitudes of the two Gaussian components to vary, since the total number of stars in the spheroid population is rather poorly known. The minimum chi-squared was achieved if the extra component was assigned a mean of 74 $\mathrm{km\,s^{-1}}$ and a sigma of 34 $\mathrm{km\ s^{-1}}$. The number of stars assigned to the spheroid population, 153, was very close to the 174 that were calculated from our standard galaxy model, giving us added confidence in that estimate. The thinner black curve in Figure 2 shows the extra distribution of stars, and the thicker black curve shows the sum of the extra stars with the standard model. The thick black curve shows reasonable agreement with the data.

One could imagine adjusting each of the model parameters (i.e. increase the normalization of the halo component), or adding additional model components (i.e. a second inner halo or metal weak thick disk component) in an attempt to fit the data without the need for this "extra" component. However, one must keep in mind the following points when imagining an expanded model:

(1) We do not expect *any* thin disk stars in our spectroscopic sample, even if we tweak the scale lengths and normalization to other components within reasonable bounds. Warps or flares of a thin (or thick disk) do not work, as they do not provide enough stars this far from the Galactic center. A spiral arm at this distance from the Sun would be 4 kpc above the Galactic plane.

(2) The velocity dispersion of the star sample is *much* narrower than that of the power law spheroid, and is significantly smaller than the local thick disk velocity dispersion.

If one wanted to fit the radial velocity distribution with a smooth distribution of stars, then a distribution with much larger scale lengths than the thick disk would be required (scale height 2 kpc, scale length 8 kpc, as described in Paper II). However, larger scale lengths generally lead to larger dispersions, which makes the agreement with the data in this respect problematic.

We will show in the next section that a typical instrumental error in the radial velocity dispersion for this data is $\sigma = 20\,\mathrm{km\ s^{-1}}$. Using this, we estimate that the intrinsic velocity dispersion of this extra component is $27\,\mathrm{km\,s^{-1}}$. The mean radial velocity of this component is $74\ \pm 5\,\mathrm{km\ s^{-1}}$. The error in mean is calculated from the uncorrected dispersion divided by the square root of the number of measured stars in that component and including the 4 $\mathrm{km\,s^{-1}}$ plate-to-plate absolute error (see §4 below) in quadrature.

Because the stars are at $l = 198°$, relatively near the anti-center, one has only a limited kinematic lever arm for interpreting radial velocities as projected circular velocities as seen from the Sun. The models in Figure 2 calculate these projections, and find that thin disk ($v_c = 220\,\mathrm{km\,s^{-1}}$) stars would have apparent radial velocities of $+49\,\mathrm{km\,s^{-1}}$, thick disk stars (rotating in a cylinder with $v_c = 170\,\mathrm{km\ s^{-1}}$) would show motions of $+54\,\mathrm{km\ s^{-1}}$ and a stationary halo would show radial velocities of $+73\,\mathrm{km\,s^{-1}}$. Any distribution of stars with significant observed mean radial velocity greater than $73\,\mathrm{km\,s^{-1}}$ which is also in a co-planar circular orbit would then be moving retrograde with respect to the disk.

These radial velocity estimates depend somewhat on our estimate of the distance to the star stream. The distance to the stream is determined from the distance modulus to the turnoff stars, which depends on the presumed absolute magnitude of these stars. The error in the distance modulus, composed of approximately equal parts error in the determination of the magnitude of the turnoff and in the error of the determination of the absolute magnitude of a turnoff star, is about 0.3 magnitudes, or 15% in distance from the sun (Paper II). The absolute magnitude of the turnoff stars was determined from the magnitude difference between the horizontal branch and main sequence stars in the same color range in the Sagittarius dwarf tidal stream (measured in SDSS filters). The result was confirmed by computing the absolute magnitudes of stars of similar color in the globular cluster Pal 5, as measured in the SDSS (Paper I). The metallicity of Pal 5 is $[Fe/H] = -1.5$, whereas the metallicity of the Sagittarius dwarf tidal stream is unknown due to age uncertainty. The Pal 5 metallicity is similar to that derived for stars on plate 797 (see §8 below) and thus the adopted distance moduli are appropriate within the quoted systematic error. The one sigma error in distance modulus gives us a distance range of 11.3 – 15.0 kpc (from the sun). There is, in addition, uncertainty in the intrinsic radial thickness of the star structure, which has approximately the same amplitude, (< 4 kpc), and is discussed below.

Since we are looking close to the Galactic anticenter, the assumed distance to the stars is of less importance. The measured circulation velocity of the stars, assuming they are in a circular orbit, is $-5\pm44\pm1\pm30 \mathrm{km s^{-1}}$, where the first error term is the one sigma contribution from the error in radial velocity determination, the second contribution to the error is from the error in distance, and the third contribution to the error is from the difference in radial velocity across the plate. For a circularly rotating group of stars, the radial velocities should shift by about 11 $\mathrm{km\,s^{-1}}$ from one side of the plate to the other side. This shift is discernable in the radial velocity data. This effect increases our measured radial velocity dispersion by a few $\mathrm{km\,s^{-1}}$. Even though formally we derive $v_c = -5 \pm 54$ $\mathrm{km\,s^{-1}}$ (no net rotation) for stars along this line of sight, we will demonstrate in §6 below that the circulation velocity of stars above the Galactic plane in this structure are consistent with a prograde rotation.

4. Standard Plate 321

Confirmation of the radial velocity zero-point and rms error in the SDSS radial velocities was determined by examining a special SDSS calibration plate. This plate, designated plate 321, specifically targeted the open cluster M67, where radial velocities are known to accuracies of 1 $\mathrm{km\,s^{-1}}$ (Mathieu et al. 1986). Exposures of 60s, 120s and 240s were obtained of this field on 2000 March 9, and processed in a manner identical to that of plate 797. The resulting 80 spectra typically have S/N of 50:1. With this large signal-to-noise ratio, the error in the radial velocities is determined from the resolution of the spectrographs and systematics of the wavelength calibration.

Figure 3 shows the difference between the SDSS radial velocities and the Mathieu et al. (1986) catalog velocities of bright blue stars in the open cluster M67 vs. the fiber number. Each plate has 640 fibers, divided into two 'left/right' halves of 320 fibers each. The SDSS instrumentation consists of a double spectrograph, with two blue and two red cameras. The fibers from the left half (numbered 1:320) of each plate are fed to one spectrograph; those from the right half (number 321:640) to another. From Figure 3 we see that there is a systematic difference of 4 $\mathrm{km\,s^{-1}}$ between the wavelength calibration on the left and right spectrographs. This difference results from separate wavelength calibrations for each spectrograph, based on arc lamp exposures before and after the target exposures. It is expected that this systematic would also be present from plate to plate, with an amplitude similar to $4\,\mathrm{km\,s^{-1}}$. This systematic is very small compared with the instrumental resolution of the SDSS spectrographs of 150 $\mathrm{km\,s^{-1}}$.

If the radial velocities of the left side of the spectrograph are adjusted by $4\,\mathrm{km\,s^{-1}}$, then the standard deviation of the radial velocity errors is $11\,\mathrm{km\,s^{-1}}$. Because the exposure times

on plate 321 are quite short, the night sky lines used to assist in setting the wavelength scale in each fiber are underexposed relative to normal SDSS plate, and thus the scatter in radial velocities can in principal be somewhat better than 11 km s^{-1} for longer exposures. The resolution and flexure of the spectrographs limits the accuracy with which we can determine radial velocities to about 7 km s^{-1} for typical SDSS exposure times. This number is derived from internal SDSS diagnostic testing.

We further check this radial velocity error empirically by using SDSS 'Quality Assurance' spectra of blue stars. 'Quality Assurance' spectra are repeats of SDSS targets previously observed on other spectroscopic plates, which are taken to assess the overall quality of the spectroscopic program. We selected 146 stellar objects with $0.15 < (g-r)_0 < 0.36$, and $18.9 < g_0 < 20$, which were observed on two different plates. Figure 4 shows the errors in radial velocity determination for these stars, which have a typical S/N of 10. The dispersion in the pairs of measurements, divided by $\sqrt{2}$, is 16 km s^{-1}; we adopt this value for correcting our observed dispersion to an intrinsic dispersion for objects with S/N ~ 10.

From these measurements, we generate a (somewhat ad hoc) formula to estimate the accuracy of individual radial velocity determinations as a function of S/N:

$$\sigma = \sqrt{7^2 + \left(\frac{150}{(S/N)}\right)^2}\ \mathrm{km\,s^{-1}}.$$

Plate 797 observations have a typical S/N of 8, rather than 10, so we adopt an instrumental spread of 20 km s^{-1} for objects on this plate when correcting the observed dispersion in Figure 2 from 34 to 27 km s^{-1}.

5. Comparison: Dispersion of stars in the Sagittarius Stream South

Since the velocity dispersion of the stars towards the anticenter is much narrower than expected for the smooth Galactic components represented at 5 kpc above the plane, we ask whether it is similar to the dispersion of a tidal stream. At least two works have estimated the dispersion within the Sagittarius dwarf tidal stream: Majewski et al. (1999) find a velocity dispersion of 27 km s^{-1}. Dohm-Palmer et al. (2001) measure a dispersion of 31 km s^{-1}.

Fortuitously, the SDSS has also obtained a sample of stellar spectra in the vicinity of the Sagittarius stream where it crosses the Celestial Equator. Sagittarius South stream stars (south here refers to south of the Galactic plane on the celestial equator, see Paper II) are seen with $10^\circ < \alpha_{2000} < 45^\circ$, $-1.5^\circ < \delta_{2000} < 1.5^\circ$ (see Figures 1 and 7 of Paper II). The turnoff of the stream is at magnitude $g \sim 21$, which is somewhat fainter than the limit

of ordinary SDSS spectra; however, we have spectra of a number of blue stars with mags $17.8 < g_0 < 20.2$ which are candidate blue horizontal branch and blue straggler stars from the Sagittarius stream. The color magnitude diagram of the stars in the direction of the Sag. south stream selected area is shown in Figure 5. The black box in the figure was used to select candidate Sagittarius stream stars with $-0.3 < (g-r)_0 < 0.2$. A histogram of the radial velocities of 306 selected stars is shown in Figure 6.

As for the data from plate 797, we show the distribution of stars expected in Figure 6 from a standard Galactic model, and fit the mean and standard deviation of the excess stars. Using the same Galactic model as for the plate 797 data, we find that there are very few thick disk stars expected in the sample (compared to the expected number of stars from the power law spheroid distribution), and a vanishingly small number of thin disk stars are expected. We did not attempt to directly calculate the normalization of the standard model star counts, since the selection function for these stars is so poorly known. However, the number of stars assigned to the smooth components using maximum likelihood techniques is similar to the number of spectra in this color and magnitude range taken from a similar area of sky at about the same Galactic latitude, but in a region that does not contain the Sagittarius stream.

As before, we fit the sum of two Gaussian distributions to the radial velocity histogram. The mean and standard deviation of the spheroid population is calculated from the model, and the sum of the number of stars in both distributions is fixed at the number of stars observed. The minimum reduced chi-squared of 1.21 was achieved with a mean radial velocity in the stream of -111 km s^{-1}, a velocity dispersion in the stream of 21 km s^{-1}, and 119 of the 306 stars assigned to the stream population. As these stars are bright, the observational error in the RVs is about 7 km s^{-1}. Correcting for this error, we quote a true dispersion of the Sag stream at this point in space of only 20 km s^{-1}. The mean radial velocity is an excellent match to the Sagittarius stream models of Ibata et al. (2001b). The dispersion of the stars observed is similar to, but even narrower than, previous determinations in the literature (which are taken at different points in the stream orbit).

6. Kinematics of the low latitude stream from other SDSS lines-of-sight

The spectroscopic observations of faint blue turnoff stars on plate 797 showed a narrow dispersion of about 27 kms^{-1} in this anti-center direction below the Galactic plane at $(l, b) = (198°, -27°)$. Assuming these stars represent a coherent structure in space and velocity, we now ask if this structure is related to the overdensities of stars detected photometrically in Paper II in several places above the Galactic plane. We address this by examining the

radial velocities of stars from SDSS (regular program) spectra which are available at low latitude in the same color-magnitude box as those of plate 797. The SDSS survey ellipse, in an attempt to avoid regions of higher than average Galactic reddening, dips down to lower Galactic latitude towards the anti-center at the beginning of most survey stripes (Stoughton et al. 2001), and this is where we find most of our spectra.

The main areas of interest where SDSS stellar spectra were available are near the areas from Paper II designated: S223+20-19.4, S183+22-19.4, and S167-54-21.5. A typical turnoff star in these structures has $g_0 = 19.4$, implying a distance to the Sun of ~ 11 kpc.

We note that Figure 16 of Paper II has an error in the labeling of the upper Figure showing S182+22-19.4. The label in the lower left corner of Figure which reads $(\alpha_{2000}, \delta_{2000}) = (125^\circ, 50^\circ)$ was improperly corrected for the off-equatorial $\cos(\delta_{2000})$ and should read $(\alpha_{2000}, \delta_{2000}) = (150^\circ, 50^\circ)$.

A color magnitude diagram of SDSS photometry of stellar objects in a box with bounds $(177^\circ < l < 193^\circ, 20^\circ < b < 30^\circ)$ is shown in Figure 7. Quasars have been rejected by using the color selection $(u-g)_0 > 0.4$. A mixture of thin and thick disk turnoff stars are seen in Figure 7 at $(g-r)_0 = 0.4$ down to magnitude about $g_0 \sim 19$. Bluer halo (spheroid) and other stars are seen to the left of this. A 'faint blue turnoff' box with $18.7 < g_0 < 20.1$ and $0.15 < (g-r)_0 < 0.36$ has been outlined with a white box on the Figure. Available SDSS spectra with photometry in this box are selected.

We were able to find three small areas of sky below Galactic latitude $l = 30^\circ$ which contained a significant number of these bluer SDSS stellar spectra. In the S223+20-19.4 region, SDSS spectra were selected in a box bounded by $130^\circ < \alpha < 136^\circ, -1.25^\circ < \delta < 3.75^\circ$. We name these groups of spectra similarly to the way we named structures in Paper II, with Galactic longitude, latitude, and turnoff magnitude: Sp225+28-19.6. Within region S183+22-19.4, we pick two sets of SDSS spectra, those in the box $179^\circ < l < 185^\circ, 25^\circ < b < 30^\circ$ are designated Sp182+27-19.4; and those in the box $185^\circ < l < 191^\circ, 21^\circ < b < 26^\circ$ are designated Sp188+24-19.3.

We also selected stellar spectra, using the same color and magnitude criteria, from the high absolute latitude field which contains the Sagittarius stream (south) as a "control." The selection region is outlined by a white box in Figure 5. Stellar spectra from this high (absolute) latitude field are selected near S167-54-21.5 in the box $25^\circ < \alpha < 50^\circ, -1.25^\circ < \delta < 1.25^\circ$. Along with the plate 797 stars with $70.5^\circ < \alpha < 73.5^\circ, -1.25^\circ < \delta < 1.25^\circ$ our sky coverage includes five areas with SDSS spectra: four at low latitude and one control field at high latitude.

Samples of spectra from each type of dataset (a plate 321 standard, a Sagittarius stream

blue horizontal branch (BHB) star, a Sp225+28-19.6 Monoceros stream turnoff star, and two stars from plate 797 at the high and low S/N limits) are presented in Figure 8. The spectra shown are smoothed over three pixels (210 km s^{-1}).

Figure 9 shows four radial velocity histograms of faint blue stars with the same colors and magnitudes as those observed on Plate 797: The upper left hand panel shows stars from Sp225+28-19.6; the upper right and lower left hand panel shows from the Sp182+27-19.4 and Sp188+24-19.3 areas, respectively, and the lower right hand panel shows those from the direction of the Sagittarius south stream. All panels except the Sagittarius panel show significant numbers of clumped radial velocities with dispersions far smaller than one expects for a spheroidal population, thus arguing that the population represented here is not associated with the stellar spheroid. Models of the expected number of stars due to the standard disks and spheroid from our Milky Way are determined in a similar fashion to that of Figure 2 and are also shown in each panel of Figure 9.

For the low latitude fields, the model predicts ten times as many halo stars as thick disk stars in each sample. In the high latitude field, it predicts a hundred times as many halo stars as thick disk stars. Therefore, we are again justified in using maximum likelihood techniques to fit only two Gaussians - one for the halo and one for the extra distribution. The technique is identical to the one used in fitting the Sagittarius stream. The mean and dispersion of the excess stars is indicated in Figure 9 and in Table 2.

The first five columns of Table 2 list the region name, right ascension and declination (J2000) of the center of the region, and Galactic l and b, for the four regions where spectra were obtained. Column six lists the average radial velocities with errors. According to the maximum likelihood fits, there were 36, 34, and 37 stars in the extra component in the Sp225+28-19.6, Sp182+27-194, and Sp188+24-19.3 directions, respectively. The errors in the average radial velocities were determined from the measured dispersion divided by the square root of the number of stars with 4 km s^{-1} plate-to-plate systematic error added in quadrature. Since the spectra in Figure 9 have a typical signal-to-noise of 10, we adopt an instrumental error in radial velocity of 16 km s^{-1}. The 1D velocity dispersions of stars in column 7 are the measured dispersion with 16 km s^{-1} subtracted in quadrature. Columns 8 and 9 list the g_0 magnitude and $(g-r)_0$ color of stars at the turnoff of the faint blue stars.

The last column of Table 2 gives the derived rotation velocity (v_c) of the group of stars in each set with errors, assuming that they are orbiting the center of the Galaxy in a circle. Although individual stars in the structure must orbit the center of mass of the Galaxy (not in cylindrical orbits), one can still use the concept of a coherent circular velocity similar to that used for the thin and thick disks. The quoted error on this circular velocity is derived by combining the following factors in quadrature: 1) A one sigma error on the observed radial

velocity; 2) A 15% error in the distance to the stars, based on uncertainty in the measured turnoff magnitude; 3) A $1^\circ - 2^\circ$ error in the position of the stars in Galactic longitude (the error due to small changes in latitude is much smaller) to allow for the fact that the region over which the stars were observed has finite size (and in fact is up to a $5^\circ \times 5^\circ$ box). The values of v_c for Galactic longitudes very near the anti-center have, of course, the largest errors; the measured circulation velocity for Sp182+27-19.4 is meaningless, since $< l >= 182^\circ$, and is not calculated. We note that the quoted v_c values are consistent within only 2.4σ of each other, suggesting that the assumption of a coherent circular velocity model is too simplistic.

In each case, rejecting now the higher absolute latitude Sagittarius stream region, we note an excess of stars clumped in radial velocity with a dispersion consistent with that of the stars on plate 797. We suggest that all these stars are related, and may be moving coherently around the Galaxy at a distance of 18 kpc from the Galactic center.

7. A Simple Low-latitude Stream Model

In order to explore the possibility that four of the regions surveyed, which differ in position on the sky by many tens of degrees and by implication many kiloparsecs, are part of one low latitude stream, we have generated a simple model which fits kinematic and photometric data in these regions of interest. The model simply integrates the equations of motion in a static potential. Two potentials were tried. The first is a logarithmic potential of the form $\Phi \sim \ln(s)$ (Richstone 1980), where $s^2 = R^2 + Z^2/q_p^2$, $R^2 = X^2 + Y^2$, q_p is the potential flattening in the Galactic rectangular coordinate system (X,Y,Z), and the Sun is at $(-8, 0, 0)$, rotating in the disk with space velocity $(10, 225, 7)\,\mathrm{km\,s^{-1}}$. The second model is the disk-halo potential of Monet, Richstone, & Schechter (1981), which also has a flattening parameter $q = 1/(1 + e)$. In this second model, q has a somewhat different interpretation than q_p; it indicates a bulge fraction in a bulge and disk system.

We experiment with different values of q_p and an initial position and velocity vector for a test particle in the proposed satellite until we achieve an orbit which both passes approximately 1 kpc closer to the plane in Z than the space locations of the four regions of interest and which also reproduces the average observed radial velocities of the turnoff stars listed in Table 2 in each of the four regions. We match our model to Z positions lower than those of our observed data to reflect the fact that we never see the peak of the star counts, which must be below our observation limits of $|b| < 15^\circ$. All these constraints are not sufficient to completely constrain the potential, given the errors, but they do provide a plausible simultaneous fit to the photometric and kinematic data in hand.

Figure 10 shows one stellar orbit which passes close to the positions of the detections of the stream at low latitude. The model parameters and goodness of the fit are listed in Table 3. In this table (x_0, y_0, z_0) and (vx_0, vy_0, vz_0) are the initial position and velocity of a star in a stream orbit. The initial position was chosen to pass through an observed piece of the stream, and the initial velocity, when integrated, minimizes the least square distances to three other positions near where data are observed while simultaneously fitting for the observed radial velocity when the stream particle makes its nearest approach over three periods.

We note here how we use the agreement in radial velocity between the model and the observations near $l = 225°$ to constrain the 'direction' of the stream. Towards $l = 225°$, the upper left hand panel of Figure 9 shows the stream stars orbiting with an average radial velocity ($103\,\mathrm{km\,s^{-1}}$) are close to that of a projected thick disk ($94\,\mathrm{km\,s^{-1}}$), and significantly far from that of a stationary halo ($143\ \mathrm{km\,s^{-1}}$). Giving this value the most weight in an averaging of the circular velocities of Table 2, we thus derive that if the structure seen in Figure 2 and the first three panels of Figure 9 are one coherent structure moving circularly then it is circling the center of the Milky Way with a systemic velocity of $110 \pm 25\ \mathrm{km\,s^{-1}}$ in the prograde direction (with the Galactic disk). The observations near $l = 180°$ are less useful because of the diminished lever arm so close to the Galactic anti-center, but are not inconsistent with this result.

The model shown here is admittedly very naive, with no tidal effects or dynamical friction included, but it does fit the observations, both in velocity and position to within the errors.

Figure 11 shows where the stars on the stream in the simple model of Table 3 would appear in the sky. This diagram is designed to be similar in appearance to those of Ibata et al. (2001b) for the Sagittarius stream. Note how this stream, which we label the Monoceros stream after the constellation in which the S225+28-19.4 region lies, remains at $|b| < 30°$ along its entire orbit. Note that elements of the stream in directions towards the Galactic center may be more difficult to detect than those towards the Galactic anticenter since they are further away from the position of the Sun, and they are at lower Galactic latitudes due to the Sun's offset from the Galactic center.

8. Discussion

We have demonstrated that there are populations of stars, with distances inferred from their turnoff magnitudes of 11 kpc from the Sun (18 kpc from the Galactic Center), that

have velocity dispersions under 30 km s^{-1}. The stars we measured, between 24° and 30° Galactic latitude, are five kpc above the Galactic plane. We have also observed a similar overdensity five kpc below the plane near the anticenter. Similar structure has been seen at every position the SDSS has observed below 30° Galactic latitude.

From the thickness of the main sequence, Paper II derived an upper limit on the radial thickness of the structure of 6 kpc as measured from the magnitude range at the turnoff. From Figure 13 of the same paper, it is shown that further down the main sequence the FWHM is 0.7 magnitudes or less. This results in an estimated thickness of the structure of 4 kpc or less. The actual thickness could be significantly smaller than this. The photometric errors in the colors of the stars could account for the entire observed width of the main sequence.

The conclusion that these observations describe a ring of stars in the plane of the Milky Way could be avoided if the distance to these stars has been grossly overestimated from the blue turnoff stars. If the absolute magnitude of these stars is not $M_g = +4.2$, but is rather $M_g = +8$, then the stars would be much closer to the Sun. At a distance of 2 kpc they could be part of a known spiral arm of the Milky Way (Quillen 2002). Similarly, if there were four magnitudes of extinction more than we expect, then dust would be confusing our distance estimates. We believe neither of these to be the case for the following reasons:

1) We know of no known star population which has the spectrum of an F star, as seen in the numerous spectra of plate 797 (see Figure 8), yet has an absolute magnitude of $M_g >> 5$.

2) The dust, if present, would redden the stars much more than is seen. The turnoff of these stars is bluer than the thick disk and if unrecognized dust were present, the stars would be much redder than $g - r = 0.3$ at turnoff.

Thus, we are left with the result that there is a ring of stars extending over at least fifty degrees of Galactic latitude near the anticenter. The detection of similar structure by Ibata et al. (2003) both above and below the plane near $(l, b) = (150°, +20°)$ and $(l, b) = (123°, -19°)$ increases the range of Galactic latitude over which the structure extends to 100° (53°, as seen from the Galactic Center).

One may estimate the metallicity of the stars in the ring from the plate 797 spectra. We use the combination of $(g - r)_0$ color and Ca II K λ 3933Å equivalent width to separate effective temperature and metallicity. Following Figure 2 of Wilhelm, Beers, & Gray (1999), we find that objects with $0.2 < (g - r)_0 < 0.3$, have an average W(K) = 4.4Å , which corresponds to an average $T_{eff} \sim 6400$ K and a typical metallicity of [Fe/H] = −1.6. The scatter is large on this metallicity (about ±0.3). The derived metallicity, which must be considered preliminary, seems reasonable, since the turnoff is bluer than thick disk stars (at

brighter g magnitude), implying that the structure has lower metallicity (or is younger). The turnoff color of the stream is the same as the stars towards the center of the Galaxy (Paper II), which we believe are spheroid stars. Since the Ca II K metallicities and turnoff colors are similar to the spheroid stars, metallicities and ages similar to spheroid stars is implied.

Using star counts, we explore the extent of the ringlike structure in more detail. In addition to the SDSS data on the Celestial Equator that was analyzed in detail in Paper II, the SDSS has obtained photometric data below 30° Galactic latitude from Galactic longitude 180° to 200° (SDSS stripes 30-37). We measured the turnoff color and magnitude of the structure in 23 pieces of sky in this general direction. Each patch of sky was $5° \times 2.5°$ and oriented along an SDSS stripe. The turnoff magnitude was determined from the peak of a plot of constant color derived from a Hess diagram such as Figure 7, and the turnoff color was determined from the peak of a plot of the number of stars versus $(g-r)_0$ color at the turnoff magnitude. The turnoff is at about $(g-r)_0 = 0.27$, with a small scatter, in all measured directions. We measured the turnoff color and magnitude in a similar region near plate 797 in the same way. The turnoff color in this direction was slightly redder, probably because of improper reddening correction in this direction (see Paper II), which has E(B-V) ~ 0.08, vs. E(B-V) ~ 0.04 for the other directions listed in Table 2 (Schlegel, Finkbeiner, & Davis 1998).

For each of these 24 datasets, we counted the number of turnoff stars. These stars were within 0.01 mag of the turnoff color in $(g-r)_0$ and within 0.275 magnitudes of the turnoff magnitude in g_0. The log of the number counts of turnoff stars vs. $Z = d\sin(b)$, where d is the distance to the ring as implied from the turnoff color and an assumed absolute magnitude of $g_0 = 4.2$ for these stars, is shown in Figure 12. We find a reasonable fit to an exponential drop off in stellar density as function of $|Z|$ at a distance of 18 kpc from the Galactic center. The scale height fit to Figure 12 is $h_Z = 1.6 \pm 0.5$ kpc, though it depends on separation of stream stars from background "spheroidal halo" stars; $h_Z = 3$ kpc is an upper limit. The blue turnoff stars disappear rapidly further than about 5 kpc above or below the Galactic plane in Z in all directions we have examined.

Five different types of symbols are used in Figure 12 to separate the stars counts into Galactic longitude bins. Though there is quite a bit of scatter in the diagram, it appears that at a fixed height above the disk, the number counts are higher at $l \sim 225°$ than they are at $l \sim 185°$ by about 25%. This effect may be simply be due to the geometry, as the fraction of the ring intercepted in each direction is different. At $l \sim 185°$, the distance to the stream (10.7 kpc) is about 12% less than that at $l \sim 225°$ (12 kpc, converting the turnoff magnitudes in Table 2 to approximate distances). Thus, the solid angle intercepted is about 25% less for the lower longitude regions, roughly consistent with the counts plotted

in Figure 12. This again argues that the structure we are seeing is coherent with relatively uniform density, at least for the northern Galactic latitudes. The planar projected distance $R = \sqrt{(X^2 + Y^2)}$ of the pieces of the structure listed in Table 2 are 19.5, 17.2, 17.8, and 17.6 kpc. The first quoted distance, to the region of Plate 797, is significantly farther than any of the other measured distances from the Galactic Center. Its turnoff color quoted in Table 2 and in Paper II is slightly bluer than that of the other structures, implying that reddening is likely to be overestimated towards this direction on the sky. Correction of this error will only increase the distance disparity between northern and southern components of the structure.

The similarity of this scale height to the proposed scale height for a metal weak thick disk (Morrison, Flynn, & Freeman 1990; Majewski 1993; Beers et al. 2002), and the embarrassingly good fit to the star number counts in Figure 20 of Paper II, made it difficult to claim that we had found a ring of stars in Paper II, even though we had observed a narrower main sequence than expected from an exponential disk. The additional evidence in the form of a narrow velocity dispersion strengthens the ring identification; the structure has a much smaller velocity dispersion than is expected for a large scale-height exponential disk.

If we identified all of the stars in this structure with an exponential disk of large scale height, then we would have been forced to include all of the stars observed towards the Galactic center in Paper II in the same disk structure, leaving no stars left in the power law spheroid distribution. That consequence of the exponential disk conclusion would have been difficult to explain, given the long history of measurements of the spheroid component. The spectra we obtained in this paper show a strong power law spheroid component near the ringlike structure, with the same density and radial velocities as standard Galactic models predict.

Still, the possibility that the stars in this Monoceros structure are related to those solar neighborhood stars called metal weak thick disk stars (Norris 1994) is intriguing. It is interesting that the inferred scale height, metallicity, and Galactic rotation speed of this population is in good agreement with those of the proposed metal-weak thick disk.

It is also interesting to compare the structure seen in the outer parts of our Galaxy to shells of stars seen in the outskirts of some elliptical galaxies. The radial narrowness of the structure (< 4 kpc), the tightness of the velocity dispersion, and the Z extent (5 kpc above and below the plane), as well as the uniform stellar population (color of turnoff and metallicity from CaII K line equivalent width) all are reminiscent of shells such as those seen in Malin & Carter (1983). If the structure is a shell, it may be possible to use the narrow velocity dispersion and Z extent to give information about an early Galactic collision with another massive object (Tremaine 1999) and to constrain the dark halo potential more

precisely (Merrifield & Kuijken 1998).

One is, of course, curious as to the total mass of the structure. We estimate lower and upper bounds on the stellar mass in the structure as follows:

A lower bound follows if the structure is two streams, and extends only as far as we see it, over an arc of 50° (rather than extending all the way around the Milky Way). In Figure 12 we fit an exponential profile to the Z extent for $15° < |b| < 30°$. The minimal star count assumes that the maximum star count (the middle of the stream) is at exactly $|b| = 15°$ so there are twice as many stars per stream as there are over the range of Galactic latitudes $15° < |b| < 30°$. In this case, we integrate the total number of F turnoff stars per square degree (as seen from the Galactic center), based on Figure 12 in this fashion:

$$N_{\rm Monoceros\ turnoff\ stars} = \frac{180°}{\pi}\frac{18{\rm kpc}}{10{\rm kpc}} \times 50° \times \frac{10000}{12.5{\rm deg}^2} \times 2 \times 2 \times \int_{15°}^{30°} e^{-d\sin|b|/h_Z} db$$

Where $180°/\pi$ handles the degrees to radians conversion; 18 kpc/10 kpc converts an angle subtended at the sun to one subtended from the Galactic center; 50° is the arc over which we actually observe Monoceros structure stars; $10000/12.5{\rm deg}^2$ are area and normalization factors; the first factor of two is for two streams, one above and one below the Galactic plane; the second factor of 2 counts the stars with $|b| < 15°$; and $d\sin|b| = |Z|$, where $d = 10$ kpc and $h_Z = 1.6$ kpc toward $l \sim 180°$. This yields $N_{MTS} = 3.6 \times 10^5$ turnoff stars. We estimate from Paper I, Paper II and Odenkirchen et al. (2001) the ratio of turnoff stars in the magnitude-color box of Figure 12 to total solar masses in stars in a globular cluster like Palomar 5 to be about 1:50. Thus the lower limit on stellar mass in the Monoceros structure is $2 \times 10^7 M_\odot$. We note that this is considerably larger than our lower limit mass from Paper II, and is based on the fact that we now have SDSS photometric data to lower $|b|$ and observe the number counts that continue to rise as $|b|$ decreases.

We follow a similar prescription in placing an upper limit, changing the 50° of arc to a full 360° and integrating from $0° < |b| < 30°$ in the above equation (removing one factor of 2). This yields $N_{MTS} = 9 \times 10^6$ and a total mass in stars of $5 \times 10^8 M_\odot$. If many stars have evaporated from the structure, or the stars are strung out over multiple orbits of the Galactic Center, then the initial stellar mass of a progenitor galaxy could be larger.

The implied rotation velocity of the stars in this structure of 110 km s^{-1} is very close to the rotation velocity of the stars that Gilmore, Wyse, & Norris (2002) attribute to the remnant of a Galactic merger which may have puffed up the thick disk, implying that the stars in our structure and the stars identified in Gilmore, Wyse, & Norris (2002) could have a common origin. If this is the case, then the merging galaxy likely had a stellar mass

substantially larger than $10^9 M_\odot$; since the Gilmore, Wyse, & Norris (2002) stars are located at 3-4 kpc from the Sun and the stars we identified are 9 kpc or more from the solar position, a common origin for the stars would imply that the stars were spread through a substantial fraction of the Galactic disk.

9. Conclusions

We find a ring of stars in the plane of the Milky Way, at a distance of 18 kpc from the Galactic Center. We have traced it from $l = 180°$ to $l = 227°$, and it may completely encircle the Galaxy at low latitudes ($|b| < 30°$). The structure extends 5 kpc above and below the plane of the Galaxy. The stars at negative Galactic latitude are about 2 kpc further from the Galactic center than those above the Galactic equator. The radial thickness of the ring is less than 4 kpc FWHM. Without more data in the plane, it is difficult to determine a scale height for the stars, but we constrain $h_Z < 3$ kpc. The stellar density at a given height above the plane is constant over the range of Galactic latitudes we have surveyed. Given that there is an asymmetry between the distance to the northern and southern portions of the structure, it is possible that there is additional substructure yet to be discovered.

The excess stars discovered at low latitudes in Paper II, and interpreted in this paper as a ring of stars, are not associated with the thin disk, thick disk, proposed metal-weak thick disk, or power law spheroid star distributions. The stars are not part of the Sagittarius dwarf tidal stream. The evidence for this includes:

(1) At distances of 5 kpc above the Galactic plane, and 18 kpc from the Galactic Center, there are no thin disk stars. Likewise, there are two orders of magnitude fewer thick disk stars than power law spheroid stars at these distances and directions.

(2) From the spectra of 327 F stars on special plate 797, we find a mean radial velocity of 74 $\mathrm{km\,s^{-1}}$ and velocity dispersion of 27 $\mathrm{km\,s^{-1}}$ for stars at $(l, b) = (198°, -27°)$. The velocity dispersion of the low latitude structure in three additional directions: $(l, b) = (225°, 28°)$, $(182°, 27.5°)$, and $(188°, 23.5°)$, are 22 $\mathrm{km\,s^{-1}}$, 30 $\mathrm{km\,s^{-1}}$, and 30 $\mathrm{km\,s^{-1}}$, respectively. Since the spectra are obtained over several degrees of sky, over which the mean radial velocity of the structure can shift, the intrinsic dispersion of the stars in the ring could be slightly smaller. These velocity dispersions are much smaller than expected from the spheroid (120 $\mathrm{km\,s^{-1}}$) or thick disk (55 $\mathrm{km\,s^{-1}}$) populations. One would expect that the proposed metal-weak thick disk with large scale height would have an even larger velocity dispersion than the thick disk, which does not match the observations. The combination of large numbers of stars at 2 – 5 kpc above the plane and a narrow velocity dispersion makes it difficult to

identify these stars with any known or proposed exponential disk distribution. No simple warp or flare of an exponential disk can simultaneously explain the excess stars above the plane and below the plane, with a velocity dispersion under 30 km s^{-1}.

(3) The narrow width of the main sequence in Hess diagrams such as Figure 7 (or Figure 12 of Paper II) is inconsistent with exponential disk models of any scale height/length, even if photometric errors are assumed to be negligible (see Figure 13 of Paper II). The photometric errors alone can explain the entire observed width of the main sequence in this diagram.

(4) The stars in Sp198-27-19.8 have Ca II 3934Å equivalent widths and $(g-r)_0$ turnoff colors which suggest metallicities of $[Fe/H] = -1.6 \pm 0.3$, consistent with stars in the halo or a metal weak thick disk, and inconsistent with those of a thin or thick disk warp or flare and also inconsistent with those of the more metal poor and bluer Sagittarius stream stars. The turnoff color is consistent with that of spheroid stars.

(5) The alignment of the density structure of the ring with the Galactic plane is inconsistent with the orbit of the Sagittarius dwarf tidal stream (which follows a nearly polar orbit).

We measure the radial velocity and velocity dispersion of the tidal stream of the Sagittarius dwarf galaxy at $(l, b) = (165°, -55°)$ to be -111 $\pm$5 km s^{-1} with a dispersion of 20 km s^{-1}. The dispersion of the Sagittarius stream is narrower than our measured dispersion for the ring of stars. If we interpret the ring of stars as the result of the tidal disruption of a smaller galaxy by the Milky Way, then this leads us to surmise that the mass of the progenitor was significantly larger than the Sagittarius dwarf galaxy.

We have estimated that there are between 3.6×10^5 and 9×10^6 turnoff stars in the ring, depending on the assumptions as to how far around the Galaxy it goes, and what its density profile is in the plane of the Milky Way. We estimated from the globular cluster Palomar 5 that the stellar mass of the structure is fifty times larger than the number of turnoff stars. Therefore, the inferred mass in stars of the ring is between 2×10^7 and $5 \times 10^8 M_\odot$. If there is a significant fraction of dark matter associated with the stars, the mass could be ten times larger. The stellar mass of the Sagittarius dwarf galaxy ($1.8 \times 10^7 M_\odot$, assuming a mass to light ratio of 1) is at the lower limit of our calculated mass range for the ring. This is consistent with our conjecture that the progenitor would be more massive than the Sagittarius dwarf from the larger measured velocity dispersion.

The radial velocities of four pieces of the ring are tabulated in Table 2. Using the simplistic assumption that the stars in the ring move coherently (on average) in a circular orbit, we calculated a prograde rotation of the ring at a speed of $110 \pm 25 km s^{-1}$. Only the first two radial velocity determinations (Sp198-27-19.8 and Sp225+28-19.6) were significant in this

calculation, since the other two directions were very close to $l = 180°$. It is interesting that the two measurements disagree at the 2.4 σ level, indicating that the kinematic and spatial structure of the ring is more complex. This is supported by the disparate Galactocentric distances measured to these two portions of the structure.

This feature of Galactic structure seen in the constellation Monoceros, confirmed here by both photometric and kinematic techniques shows the depth and accuracy of new wide area surveys such as the SDSS and provides a new set of tracers for exploring the structure and evolution of our Milky Way.

We thank Rich Kron for useful discussions. HJN acknowledges funding from Research Corporation. We thank the anonymous referee for suggestions which improved the paper.

Funding for the creation and distribution of the SDSS Archive has been provided by the Alfred P. Sloan Foundation, the Participating Institutions, the National Aeronautics and Space Administration, the National Science Foundation, the U.S. Department of Energy, the Japanese Monbukagakusho, and the Max Planck Society. The SDSS Web site is http://www.sdss.org/.

The SDSS is managed by the Astrophysical Research Consortium (ARC) for the Participating Institutions. The Participating Institutions are The University of Chicago, Fermilab, the Institute for Advanced Study, the Japan Participation Group, The Johns Hopkins University, Los Alamos National Laboratory, the Max-Planck-Institute for Astronomy (MPIA), the Max-Planck-Institute for Astrophysics (MPA), New Mexico State University, University of Pittsburgh, Princeton University, the United States Naval Observatory, and the University of Washington.

REFERENCES

Allen, C. W. 2000, in Allen's Astrophysical Quantities, ed. A. N. Cox

Alard, C. 2001, preprint astro-ph/0007013

Bahcall, J. N. & Soneira, R. M. 1984, ApJS, 55, 67

Beers, T. C., Drilling, J. S., Rossi, S., Chiba, M., Rhee, J., Führmeister, B, Norris, J. E., and von Hippel, T. 2002, AJ, 124, 931

Bellazzini, M., Ferraro, F., Ibata, R. 2002, AJ, 124, 915.

Blanton, M. R., Lupton, R. H., Maley, F. M., Young, N., Zehavi, I., & Loveday, J. 2002, AJ, in press

Chen, B. et al. 2001, ApJ, 553, 184

Dohm-Palmer, R. C., Helmi, A., Morrison, H., Mateo, M., Olszewski, E. W., Harding, P., Freeman, K.C., Norris, J., & Shechman, S. A. 2001 ApJ 555, L37

Fukugita, M., Ichikawa,T., Gunn, J. E., Doi, M., Shimasaku, K., Schneider, D. P. 1996, AJ, 111, 1758

Gilmore, G., Wise, R. F. G., & Norris, J. E. 2002, ApJ, 574, L39

Gilmore, G., and Wyse, R. F. G. 1985, AJ, 90, 2015

Gunn, J. E. et al. 1998, AJ, 116, 3040

Helmi, A., White, S. D. M., de Zeeuw, P. T., and Zhao, H. 1999, Nature, 402, 53

Hogg, D. W. , Finkbeiner, D. P., Schlegel, D. J., & Gunn, J. E. 2001, AJ, 122, 2129

Ibata, R., Irwin, M., Lewis, G. F., Stolte, A. 2001a, ApJ, 547, L133

Ibata, R., Lewis, G. F., Irwin, M., Totten, E., and Quinn, T. 2001b, ApJ, 551, 294

Ibata, R. A., Irwin, M. J., Lewis, G. F., Ferguson, A. M. N., and Tanvir, N. 2003, MNRAS, in press (astro-ph/0301067)

Kundu, A., et al. 2002, ApJ, 576, L125

Larsen, J. A., & Humphreys, R. M. 1996, AJ, 468, 99

Lupton, R. H., et al., AJ, in preparation

Majewski, S. R., Siegel, M. H., Kunkel, W. E., Reid, I. N., Johnston K. V., Thompson, I. B., Landolt, A. U., and Palma, C. 1999, AJ, 118, 1709

Majewski, S. R., Munn, J., A., and Hawley, S. L. 1996, ApJ, 459, L73

Majewski, S. R. 1993, ARA&A, 31, 575

Malin, D. F. & Carter, D. 1983, ApJ, 274, 534

Martinez-Delgado, D., Aparicio, A., Gomez-Flechoso, M. Angeles, & Carrera, Ricardo 2001, ApJ, 549, L199

Mateo, M., Olszewski, E. W., & Morrison, H. 1998, ApJ, 508, L55

Mathieu, R. D., Latham, D. W., Griffin, R. F., & Gunn, J. E. 1986, AJ, 92, 1100

Merrifield, M. & Kuijken, K. 1998, MNRAS, 297, 1292

Monet, D. G., Richstone, D. O, & Schechter, P. 1981, ApJ, 245, 454

Morrison, H. L., Flynn, C., & Freeman, K. C. 1990, AJ, 100, 1191

Newberg, H., Yanny, B., et al. 2002, ApJ, 569, 245 (Paper II)

Norris, J. E. 1994, ApJ, 431, 645

Norris, J., Bessell, M. S., & Pickles, A. J. 1985, ApJS, 58, 463

Odenkirchen, M. et al. 2001, ApJ, 548, L165

Parker, J. E., Humphreys, R. M., and Larsen, J. A. 2001, BAAS, 199, #91.05

Pier, J. et al. 2002, AJ, 125, 1559.

Quillen, A. C. 2002, AJ, 124, 400

Richstone, D. O. 1980, ApJ, 238 , 103.

Rockosi, C. M. et al. 2002, AJ, 124, 349

Schlegel, D.J., Finkbeiner, D.P., & Davis, M. 1998, ApJ, 500, 525

Smith, J. A. et al. 2002, AJ, 123, 2121

Stoughton, C., et al. 2001, AJ, 123, 485

Tremaine, S. 1999, MNRAS, 307, 877

Vivas, A. K. et al. 2001, ApJ, 554, L33

Wilhelm, R., Beers, T., Gray, R. O. 1999, AJ, 117, 2308

Yanny, B., Newberg, H. J., et al. 2000, ApJ, 540, 825 (Paper I)

York, D.G. et al. 2000, AJ, 120, 1579

Fig. 1.— A $g_0, (g-r)_0$ color magnitude diagram of SDSS stars near $(l, b) = (198°, -27°)$. The Milky Way's thick disk turnoff is seen as a wide structure near $(g-r)_0 = 0.3, g_0 = 19$. Note, however, the additional faint turnoff at $(g-r)_0 = 0.2,\ g_0 = 19.5$. This is where the spectroscopic targets for plate 797 observations were selected (triangles).

Fig. 2.— Histogram of radial velocities for 327 blue stars with $19.1 < g_0 < 20.3$ and $0.158 < (g-r)_0 < 0.3$ in the direction $(l, b) = (198°, -27°)$. The stars have an average heliocentric radial velocity of 74 $\mathrm{km\,s^{-1}}$ with a remarkably small 1D velocity dispersion of $\sigma = 27 \mathrm{km s^{-1}}$ after subtraction in quadrature of typical instrumental errors of $20 \mathrm{km s^{-1}}$. The distance to the stars was calculated from the turnoff magnitude listed in Table 2, assuming an absolute magnitude of $M_g = 4.2$ for turnoff stars. Also plotted are several models, representing expected contributions and projected radial velocities of stars from the Milky Way's thin disk (red) and thick disk (green), both negligible, for objects of this color at this distance from the Galactic center, and for the stellar spheroidal halo (blue). The black dotted line is the sum of the thin disk, thick disk and halo components and the thin solid line represents a Gaussian fit to the 'extra' stars, where the contribution of the halo has been adjusted to minimize the overall fit (thick black line). The density excess and narrow dispersion are striking for these stars, which are apparently 20 kpc from the Galactic center.

Fig. 3.— The difference of SDSS radial velocities and catalog velocities (Mathieu et al. 1986) of bright blue stars in the open cluster M67 vs. the fiber number on SDSS plate 321. Each plate has 640 fibers, divided into two (left and right) halves of 320 fibers each. The wavelength calibrations are determined separately for the left and right halves based on arc lamp exposures before and after the target exposures. There is a systematic difference in the SDSS velocities on the left and right halves of the plate of amplitude $4 \mathrm{km\,s^{-1}}$; this is an estimate of the absolute error in radial velocities determined throughout this paper. The one sigma dispersion of 11 $\mathrm{km\,s^{-1}}$ is a measure of the rms scatter for individual measurements of bright star radial velocities. For lower S/N observations, such as those in plate 797, we estimate a one sigma dispersion of 20 $\mathrm{km\,s^{-1}}$.

Fig. 4.— Histogram of errors in the determination of radial velocities for all SDSS spectra from many plates in the color-magnitude box of: $0.15 < (g-r)_0 < 0.36; 18.9 < g_0 < 20.0$. These are differences in the automated radial velocities determined for multiple SDSS observations of the same star on different spectroscopic plates. There are N=146 pairs, with $\sigma/\sqrt{2} = 16.3$ $\mathrm{km\,s^{-1}}$, which gives us a good estimate of our radial velocity accuracy for objects with typical S/N=10.

Fig. 5.— The color magnitude ("Hess") diagram of SDSS stars in the region of the Sagittarius

stream near $(l, b) = (165°, -55°)$. The greyscale in each color-magnitude pixel is proportional to the square root of the number of stars in that bin. The black box indicates the area where horizontal branch and blue straggler stars from the Sagittarius stream are found. The white box matches the selection box used at lower Galactic latitudes and represents a high-latitude control field for determining the extent of the low latitude blue stream stars. Objects in the figure were selected with the color cuts: $0.4 < (u-g)_0 < 1.8, -1 < (g-r)_0 < 1.5$.

Fig. 6.— Histogram of radial velocities for very blue horizontal branch and blue straggler stars in the direction of the Sag South stream (black box of Figure 5). The stars have an average heliocentric radial velocity of $-111\,\mathrm{km\,s^{-1}}$ and a velocity dispersion of $\sigma \sim 20\,\mathrm{km\,s^{-1}}$, (after removing an instrumental spread of $7\mathrm{km\,s^{-1}}$). consistent with models of the Sagittarius South tidal stream.

Fig. 7.— The color magnitude density diagram of SDSS imaging (all stellar objects) in the a region surrounding the areas Sp182+27-19.4 and Sp188+24-19.3 centered on $(l, b) = (185°, 25°)$. The greyscale in each color-magnitude pixel is proportional to the square root of number of stars in that bin. The white box indicates the selection area used for picking SDSS spectra of stars in the faint blue turnoff. Objects in the whole figure were selected with the color cuts: $0.4 < (u-g)_0 < 1.8, -1 < (g-r)_0 < 1.5$.

Fig. 8.— Five SDSS spectra plotted in the wavelength range 3850–5000Å (the full SDSS spectra extend over the range 3780–9100Å). All spectra are offset and scaled to fit on the page, with a zero flux level drawn under each and a vertical reference line at H-beta. Top to bottom: A G star in the M67 standard plate 321 field; A BHB star in the Sagittarius dwarf southern tidal stream; An F turnoff star in the Sp225+28-19.6 area of Monoceros; and two plate 797 stars representing the bright and faint ends of the set of F turnoff stars observed spectroscopically.

Fig. 9.— Histograms of radial velocities, with Galactic model fits, for the spectra of stars of the last four entries of Table 2. The distance to the stars was calculated from the turnoff magnitude listed in Table 2, assuming an absolute magnitude of $M_g = 4.2$ for turnoff stars. The central velocities and velocity dispersions of three low latitude panels are consistent with one tidal stream circling the Galaxy at a distance of 18 kpc from the Galactic center. The dispersion of the stream is consistent with the 27 $\mathrm{km\,s^{-1}}$ seen in Figure 2. The lower right panel shows that the low latitude structure seen in the other panels is not present at Galactic latitude $b \sim -55°$.

Fig. 10.— Galactic (X,Y,Z) plane projection plots of one possible orbit for stars in the stream. This sample model has parameters listed in Table 3. The Galactic center and Sun at (X,Y,Z) = (-8,0,0) kpc are marked. The four spots at R $\sim$ 18 kpc from the G.C. are

where the SDSS has photometric and kinematic data showing a faint blue turnoff. The radial velocity of the sample orbit matches that observed at the four observed regions to within about 7 $\mathrm{km\,s^{-1}}$ (see Table 3). The model has a flattened logarithmic potential with potential flattening parameter of $q_p = 0.69$.

Fig. 11.— Equatorial $(\alpha_{2000}, \delta_{2000})$ Aitoff projection plot of one possible orbit of the stream (from Table 3). The stars are all at about 18 kpc from the Galactic center, and are nearly all at $|b| < 30^\circ$ (bounded by red lines). The color of the plotted orbit changes as noted in the figure legend to represent projected heliocentric radial velocity for stars observed from the Sun. The four black points are the positions of the observed SDSS spectroscopic and photometric data. The black points are offset a bit from the stream centers to reflect the fact that the data do not probe to $|b| < 15^\circ$. A shift of about about 1 kpc is assumed. The stripes of the SDSS survey area (as planned), are plotted in magenta. Only every other stripe in the Northern Galactic hemisphere is plotted.

Fig. 12.— Height above (or below) the plane $|Z|$ vs. turnoff faint blue star counts in a color magnitude box for stars near the turnoff if 12.5 $\mathrm{deg^2}$ boxes in the low latitude stream. Though the estimate of background (smooth stellar halo stars) is uncertain, one can fit an exponential profile to the density of stars in the stream vs. height above the disk in the range where data is available. This fit yields a formal scale height of $h_Z = 1.6 \pm 0.5$ kpc for this choice of constant (700) background counts. The data points are broken into Galactic longitude ranges.

Table 1. Blue stars near (l,b) = (198, -27) (Table Stub only)

R.A. °	Dec. °	SDSS ID r-re-c-f-id	Fiber ID plate-mjd-fiber	g_0 mag	$(g-r)_0$ mag	$(u-g)_0$ mag	RV km s^{-1}	W_K Å	color flag	E(B-V) mag
70.598290	-0.213427	0125-7-3-546-0318	797-52263-318	19.632	0.232	0.984	30.1	6.19	1	0.0606
70.603553	-0.237871	0125-7-3-546-0219	797-52263-313	19.919	0.280	0.731	62.9	3.36	1	0.0573
70.622982	0.047201	0125-7-4-546-0262	797-52263-359	19.788	0.264	0.708	89.0	5.01	1	0.0768
70.625600	-0.057840	1752-0-3-332-0329	797-52263-358	19.230	0.272	1.042	78.4	4.11	1	0.0798
70.652157	-0.544781	1752-0-2-333-0301	797-52263-311	19.397	0.223	0.892	145.5	3.76	1	0.0346
70.788270	0.555787	0125-7-5-547-0374	797-52263-339	19.229	0.138	1.122	77.0	5.03	0	0.0788

Table 2. Summary of Stream detection pieces

Name	α	δ	l	b	$< v_R >$	$\sigma(v_R)$	g_0[1]	$(g-r)_0$[1]	v_{circ}
Sp198-27-19.8[2]	72	0	198	-27	74 ±5	27	19.8	0.24	-5±54
Sp225+28-19.6	133	2	225	28	103 ±6	23	19.6	0.26	139±27
Sp182+27-19.4	117	38	182	27	22 ±8	30	19.4	0.28	—
Sp188+24-19.3	115	32	188	24	34 ±7	30	19.3	0.28	12±200
Sag. South Strm	35	0	165	-55	-111 ±5[3]	20[3]	21.5[3]	0.22[3]	—

[1]mag and color of faint blue Monoceros turnoff except where indicated

[2]Plate 797

[3]For the Sagittarius stream, this $< v_R >$ and σ refer to Sagittarius stream blue horizontal branch and blue straggler stars rather than those in the Monoceros structures. The color and mag are those of the Sag. stream.

Table 3. Stream Model parameters

Parameter	Value
Halo Potential model 1	ln(s)
Potential Flattening for model 1	$q_p = 0.69$
Halo Potential model 2	Monet, Richstone, & Schechter
Potential Flattening for model 2	$q = 0.78$
(x_0, y_0, z_0)	$(-15.498, -7.487, 4.633)$ kpc
(vx_0, vy_0, vz_0)	$(-83.6, 202.4, 59.4)$ km s^{-1}
Period	600 Myr
Semi-Major Axis of Orbit	18 kpc
Predicted (Observed) RV at Sp225+28-19.6	96 (103) km s^{-1}
Predicted (Observed) RV at Sp198-27-19.8	72 (74) km s^{-1}
Predicted (Observed) RV at Sp182+27-19.4	25 (22) km s^{-1}
Predicted (Observed) RV at Sp188+24-19.3	36 (34) km s^{-1}
Closest approach of orbit to Sp198-27-19.8	0.6 kpc [1]
Closest approach of orbit to Sp182+27-19.4	0.7 kpc [1]
Closest approach of orbit to Sp188+24-19.3	0.3 kpc [1]

[1]The closest approach is actually to a position 1 kpc lower in $|Z|$ to that of the observed stars.

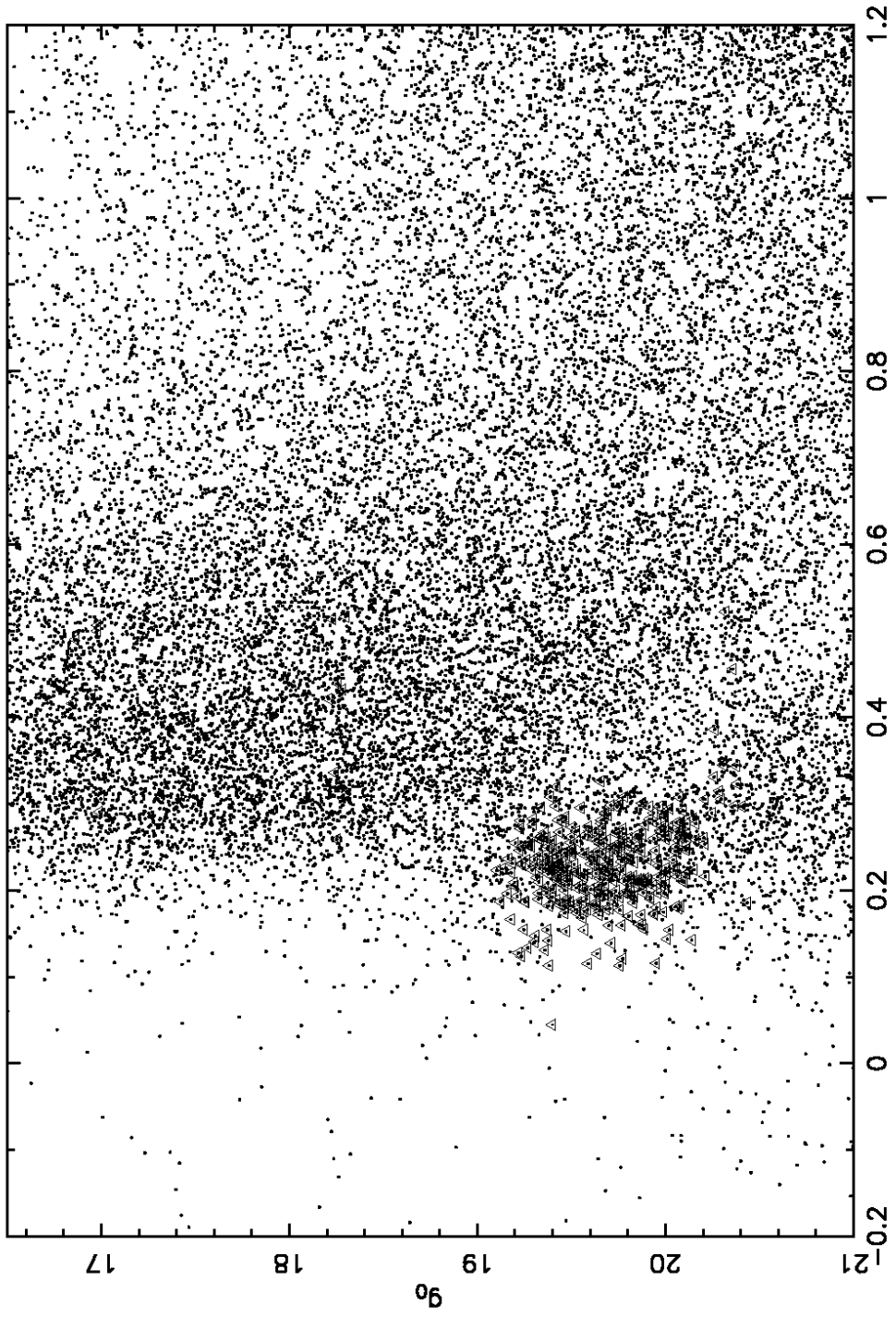
17
18
19
20
21
g_0
−0.2
0
0.2
0.4
0.6
0.8
1
1.2
$(g-r)_0$

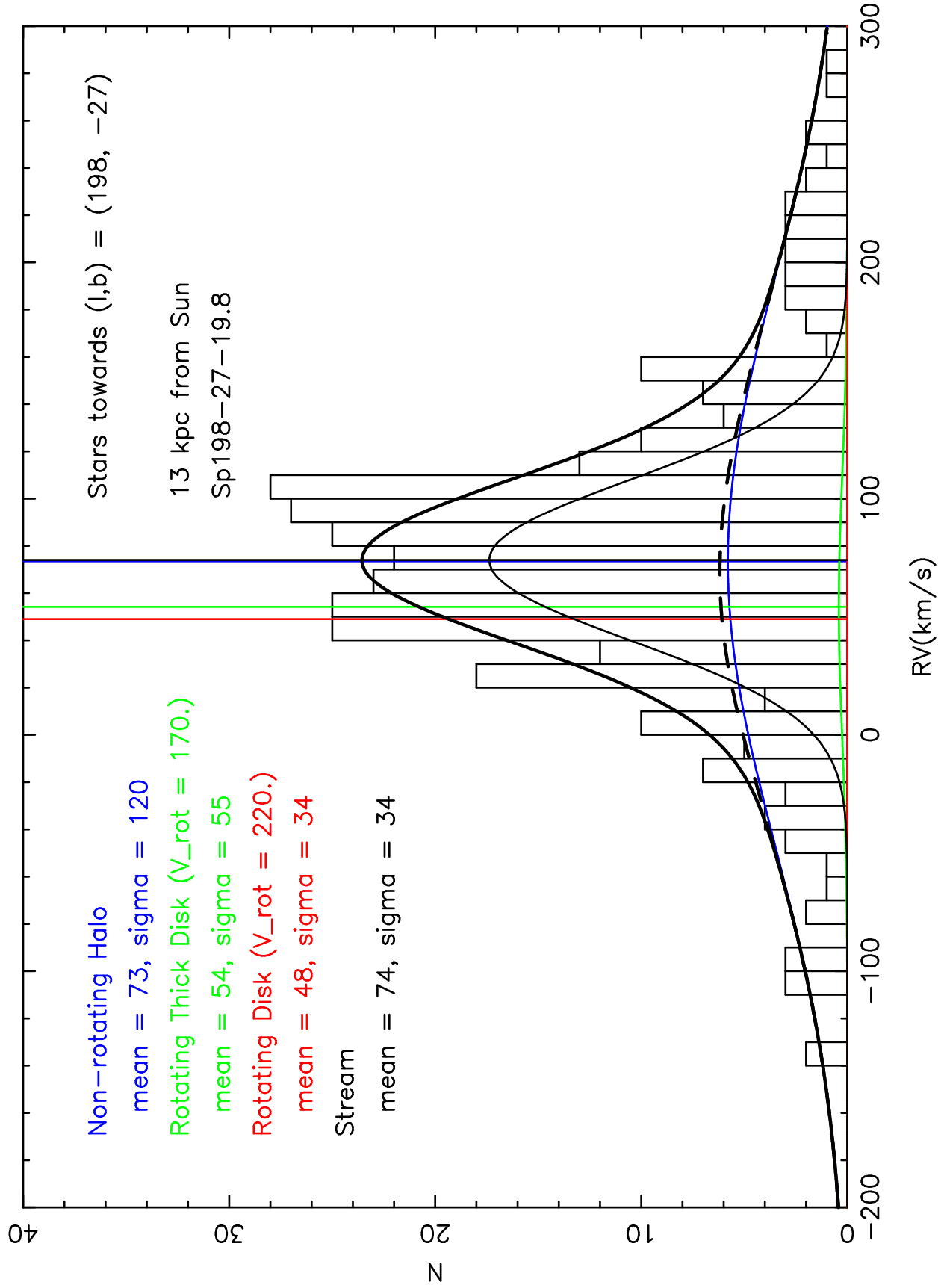
Stars towards (l,b) = (198, −27)
13 kpc from Sun
Sp198−27−19.8
Non−rotating Halo
mean = 73, sigma = 120
Rotating Thick Disk (V_rot = 170.)
mean = 54, sigma = 55
Rotating Disk (V_rot = 220.)
mean = 48, sigma = 34
Stream
mean = 74, sigma = 34
N
RV(km/s)
0
10
20
30
40
−200
−100
0
100
200
300

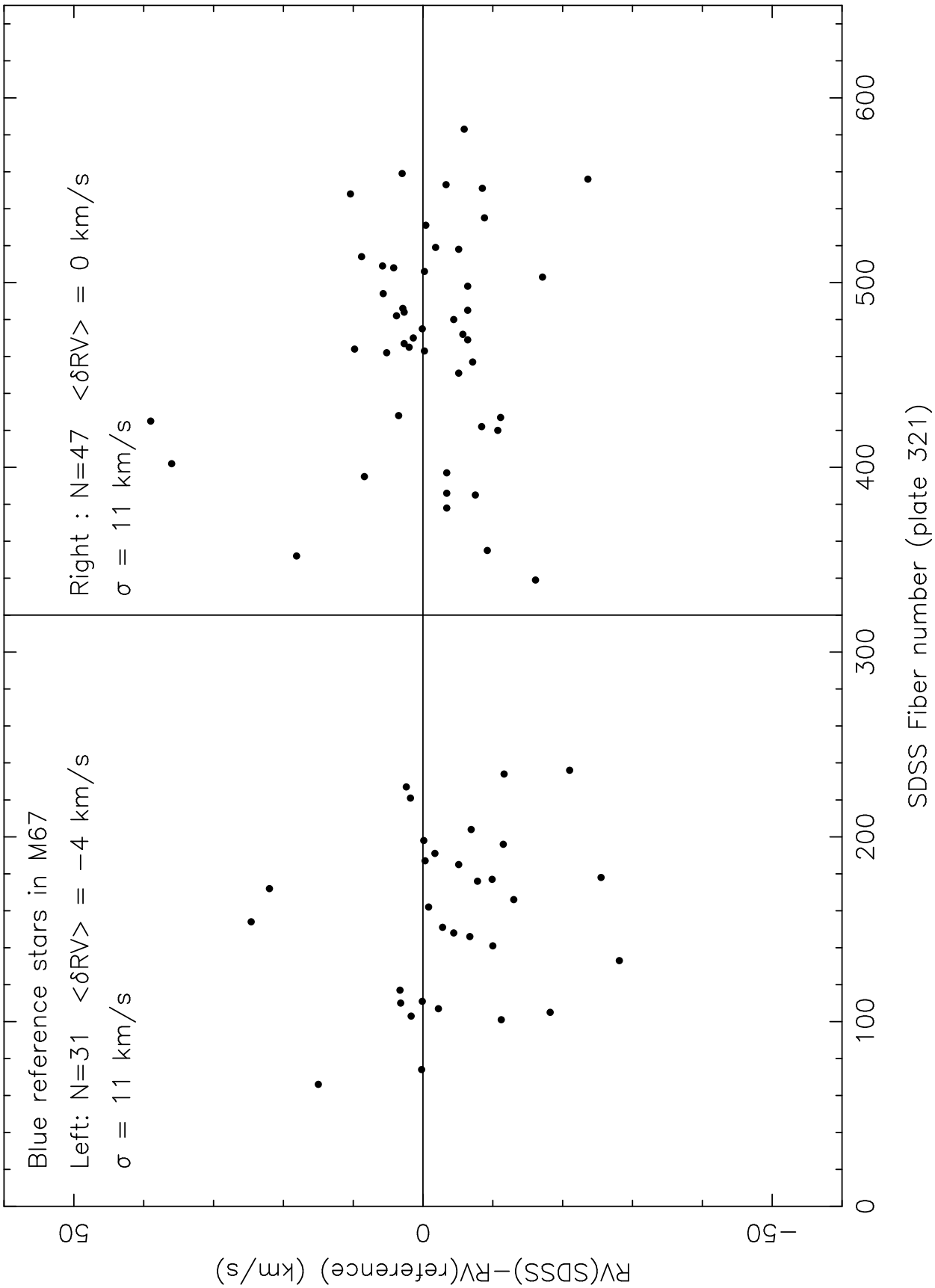
Blue reference stars in M67
Left: N=31 <δRV> = −4 km/s
σ = 11 km/s
Right : N=47 <δRV> = 0 km/s
σ = 11 km/s
RV(SDSS)−RV(reference) (km/s)
SDSS Fiber number (plate 321)
50
0
−50
0
100
200
300
400
500
600

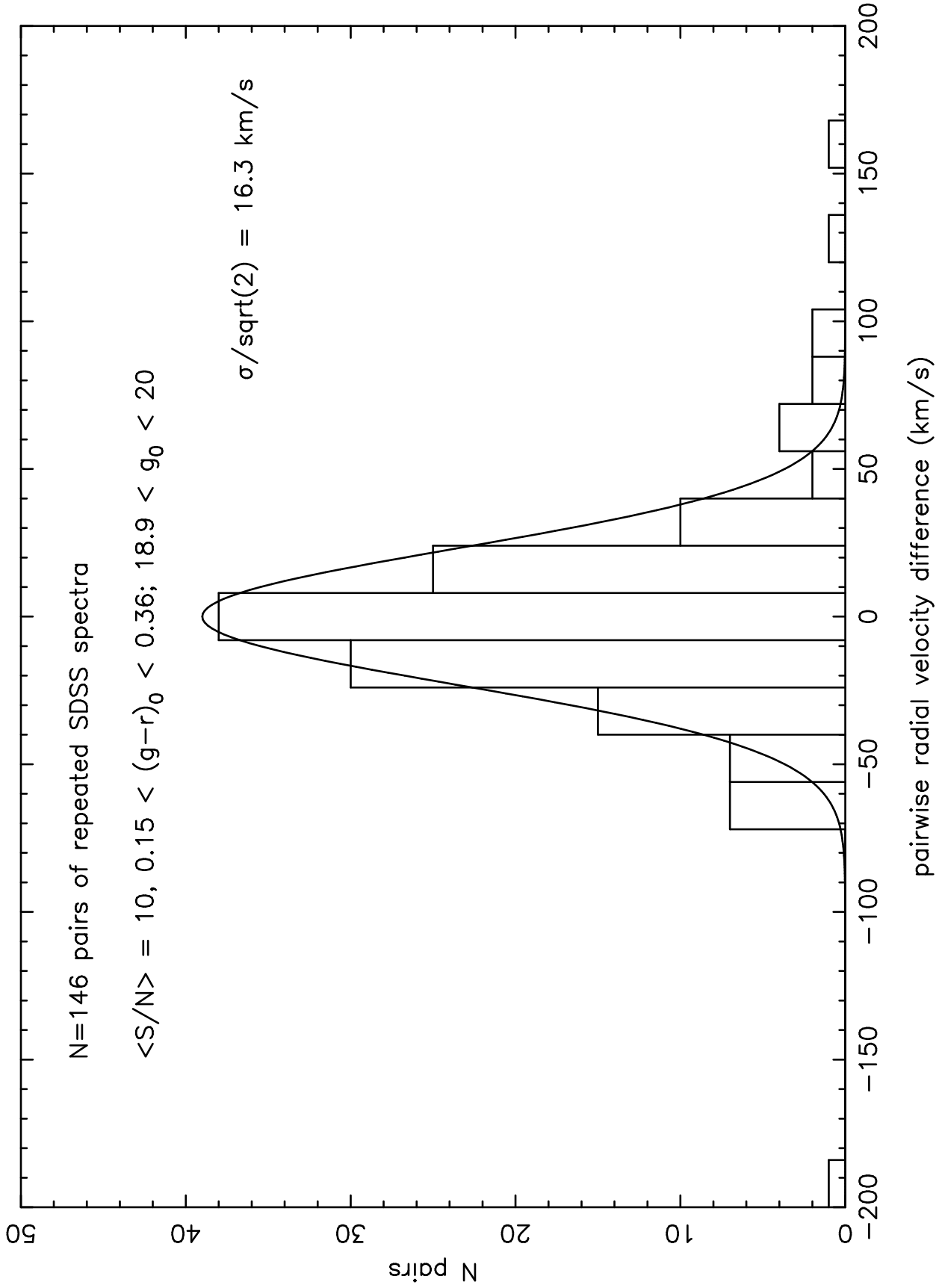
N pairs
pairwise radial velocity difference (km/s)
N=146 pairs of repeated SDSS spectra
<S/N> = 10, 0.15 < (g−r)0 < 0.36; 18.9 < g0 < 20
σ/sqrt(2) = 16.3 km/s
0
10
20
30
40
50
−200
−150
−100
−50
0
50
100
150
200

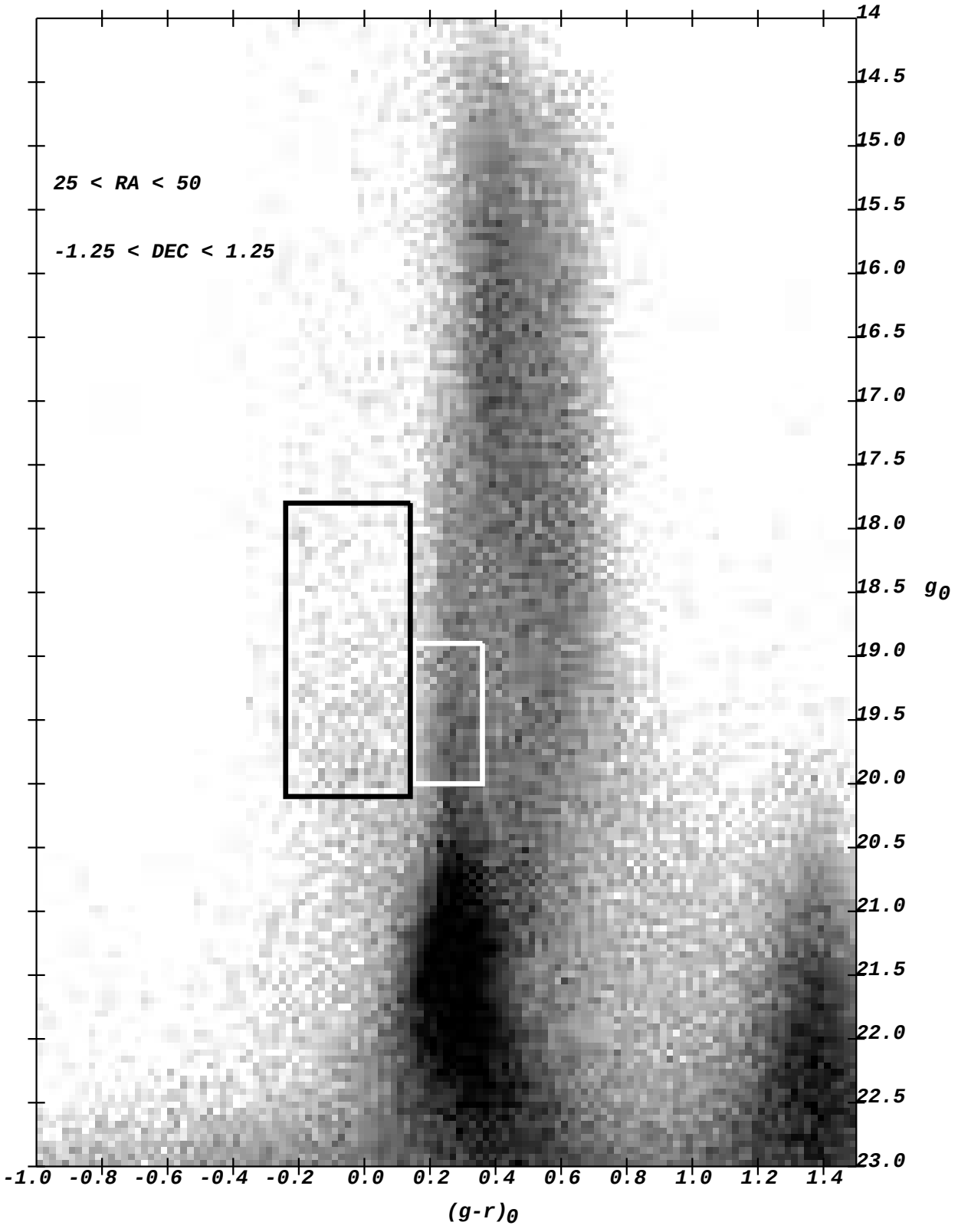
25 < RA < 50
-1.25 < DEC < 1.25
14
14.5
15.0
15.5
16.0
16.5
17.0
17.5
18.0
18.5
19.0
19.5
20.0
20.5
21.0
21.5
22.0
22.5
23.0
g_0
-1.0
-0.8
-0.6
-0.4
-0.2
0.0
0.2
0.4
0.6
0.8
1.0
1.2
1.4
$(g-r)_0$

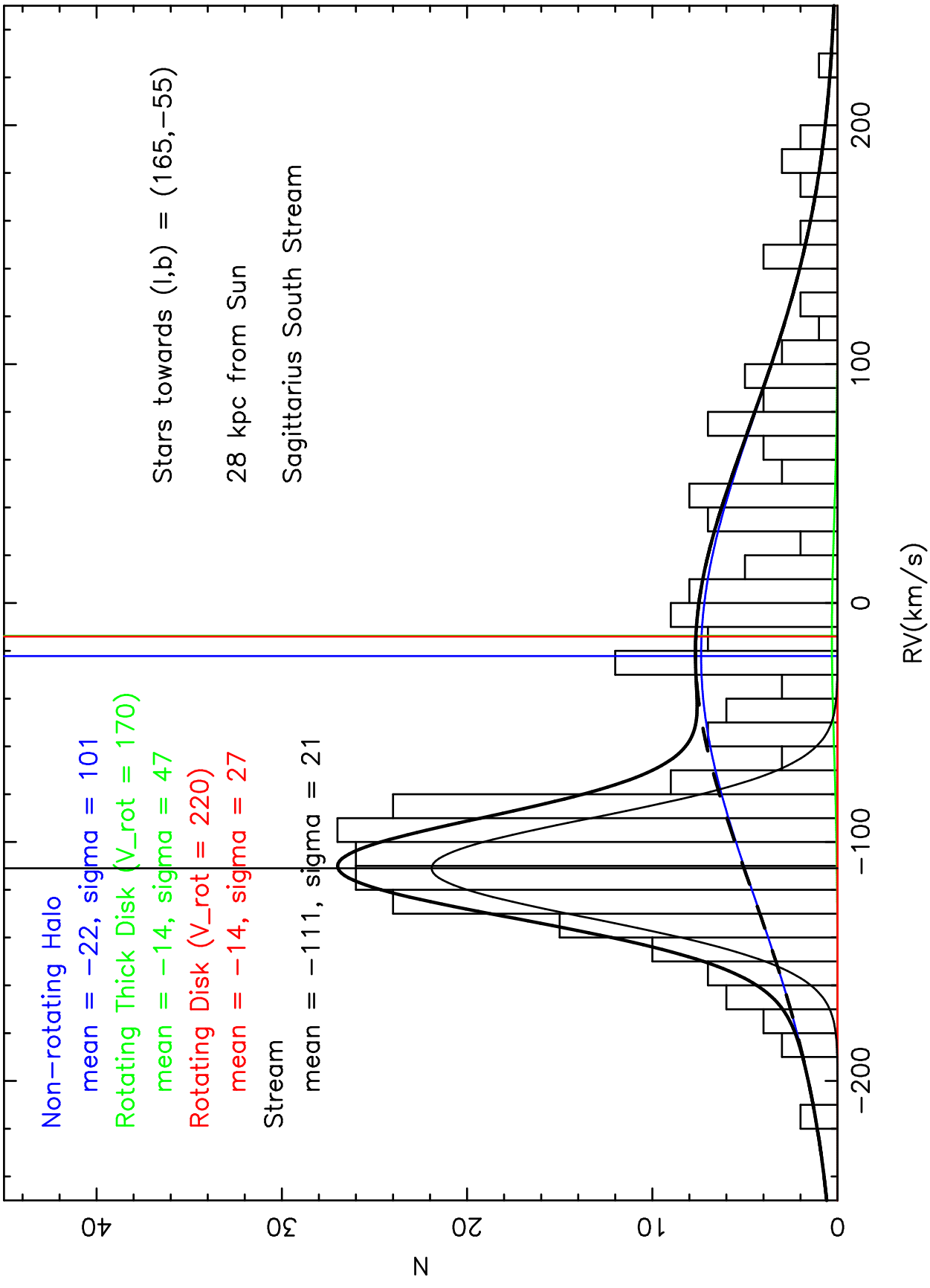
Stars towards (l,b) = (165,−55)
28 kpc from Sun
Sagittarius South Stream
Non−rotating Halo
mean = −22, sigma = 101
Rotating Thick Disk (V_rot = 170)
mean = −14, sigma = 47
Rotating Disk (V_rot = 220)
mean = −14, sigma = 27
Stream
mean = −111, sigma = 21
N
RV(km/s)
0
10
20
30
40
−200
−100
0
100
200

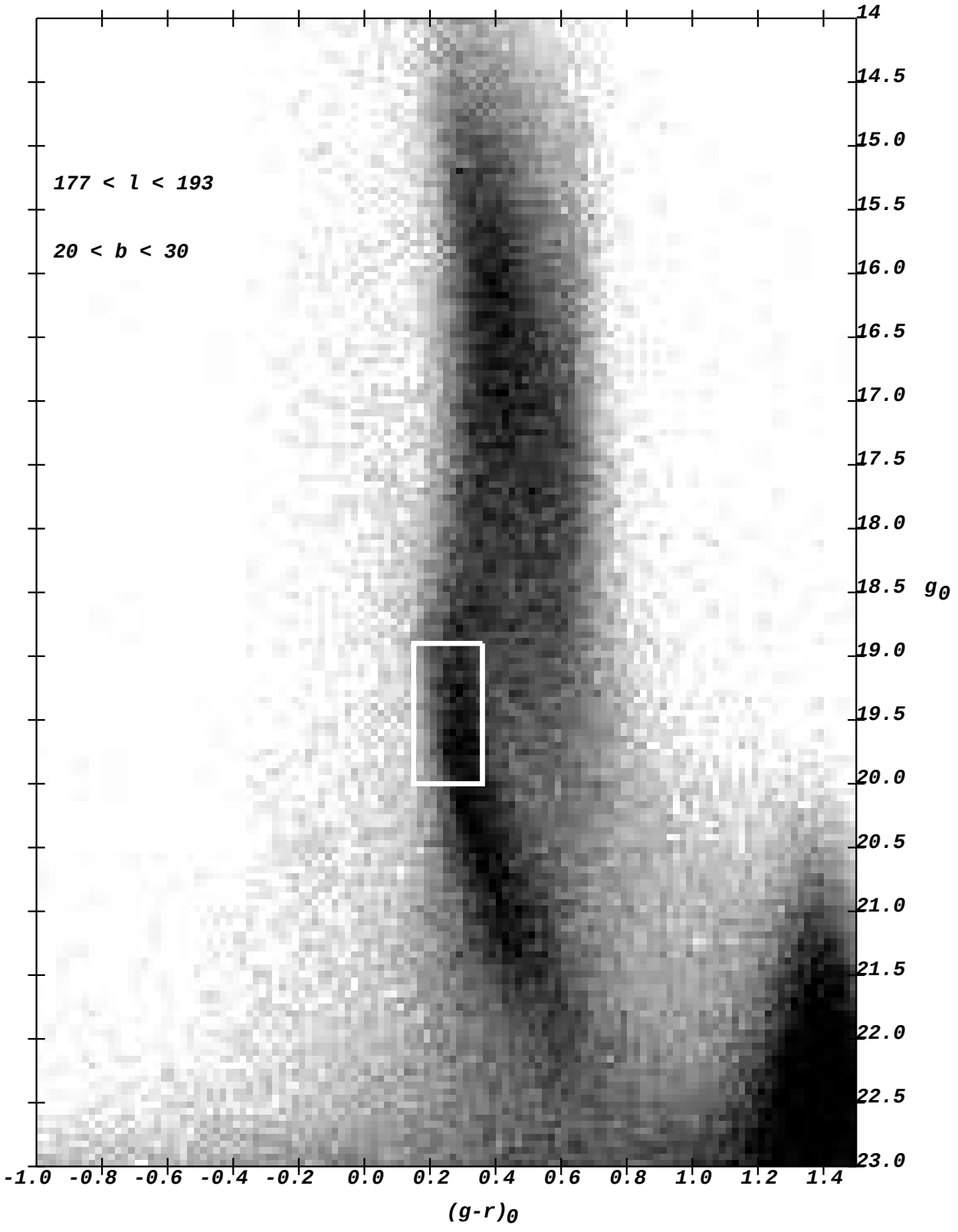
177 < l < 193
20 < b < 30
14
14.5
15.0
15.5
16.0
16.5
17.0
17.5
18.0
18.5
19.0
19.5
20.0
20.5
21.0
21.5
22.0
22.5
23.0
g0
-1.0
-0.8
-0.6
-0.4
-0.2
0.0
0.2
0.4
0.6
0.8
1.0
1.2
1.4
(g-r)0

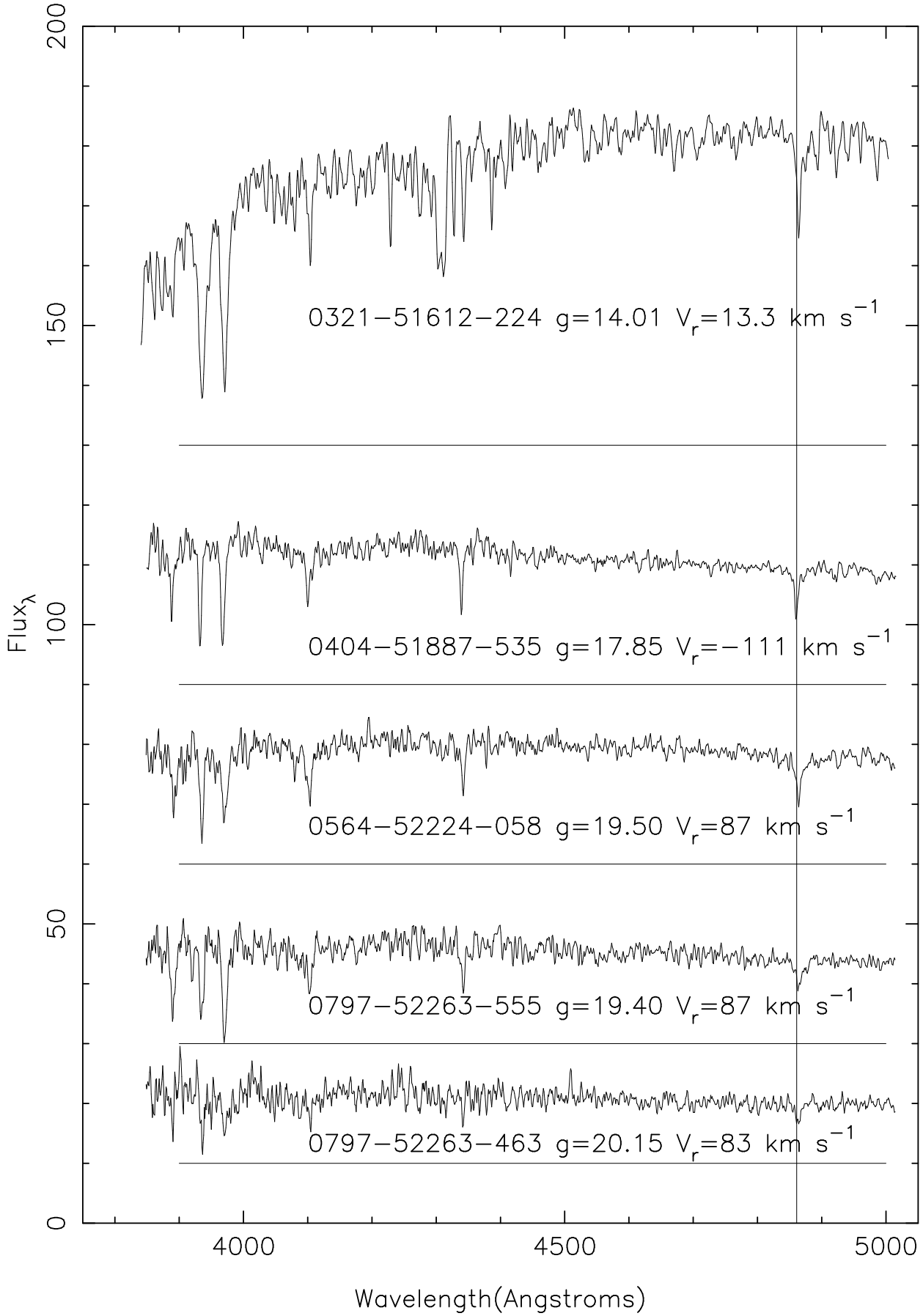
0321−51612−224 g=14.01 V_r=13.3 km s^-1
0404−51887−535 g=17.85 V_r=−111 km s^-1
0564−52224−058 g=19.50 V_r=87 km s^-1
0797−52263−555 g=19.40 V_r=87 km s^-1
0797−52263−463 g=20.15 V_r=83 km s^-1
Flux_λ
Wavelength(Angstroms)
0
50
100
150
200
4000
4500
5000

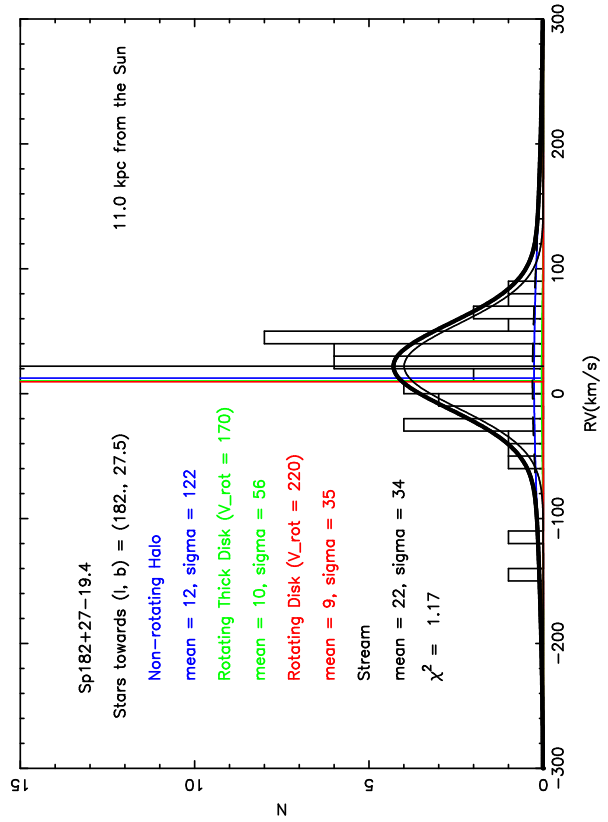
Sp182+27−19.4
Stars towards (l, b) = (182., 27.5)
11.0 kpc from the Sun
Non−rotating Halo
mean = 12, sigma = 122
Rotating Thick Disk (V_rot = 170)
mean = 10, sigma = 56
Rotating Disk (V_rot = 220)
mean = 9, sigma = 35
Stream
mean = 22, sigma = 34
χ² = 1.17
N
RV(km/s)

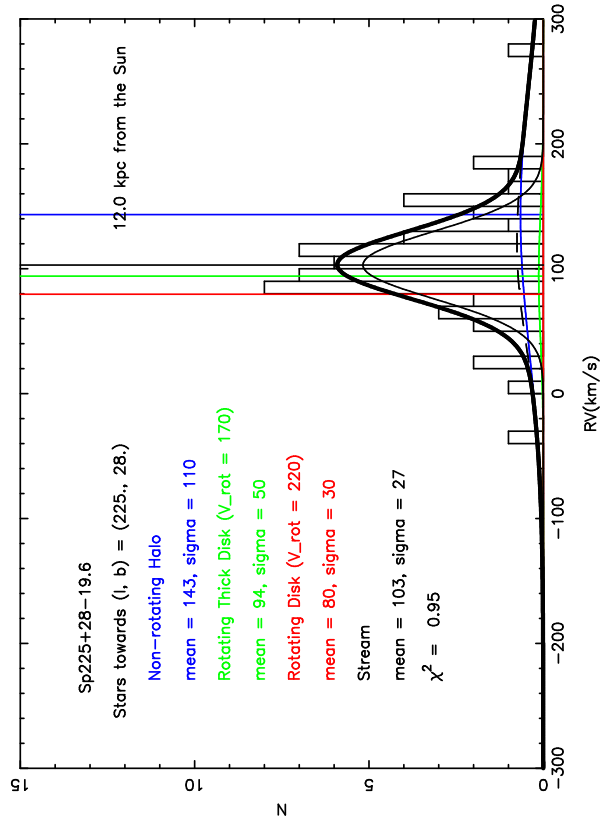
Sp225+28−19.6
Stars towards (l, b) = (225., 28.)
12.0 kpc from the Sun
Non−rotating Halo
mean = 143, sigma = 110
Rotating Thick Disk (V_rot = 170)
mean = 94, sigma = 50
Rotating Disk (V_rot = 220)
mean = 80, sigma = 30
Stream
mean = 103, sigma = 27
χ² = 0.95
N
RV(km/s)

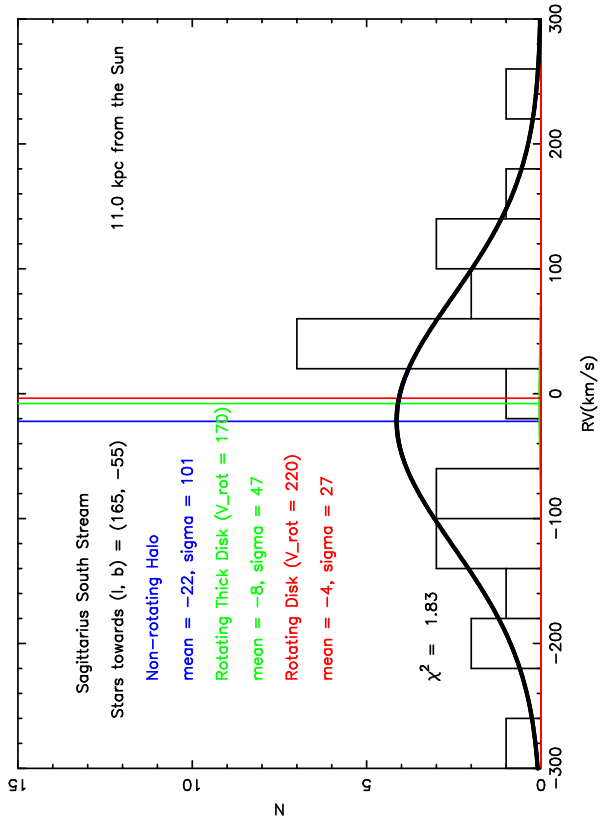
Sagittarius South Stream
Stars towards (l, b) = (165, −55)
11.0 kpc from the Sun
Non−rotating Halo
mean = −22, sigma = 101
Rotating Thick Disk (V_rot = 170)
mean = −8, sigma = 47
Rotating Disk (V_rot = 220)
mean = −4, sigma = 27
χ² = 1.83
N
RV(km/s)

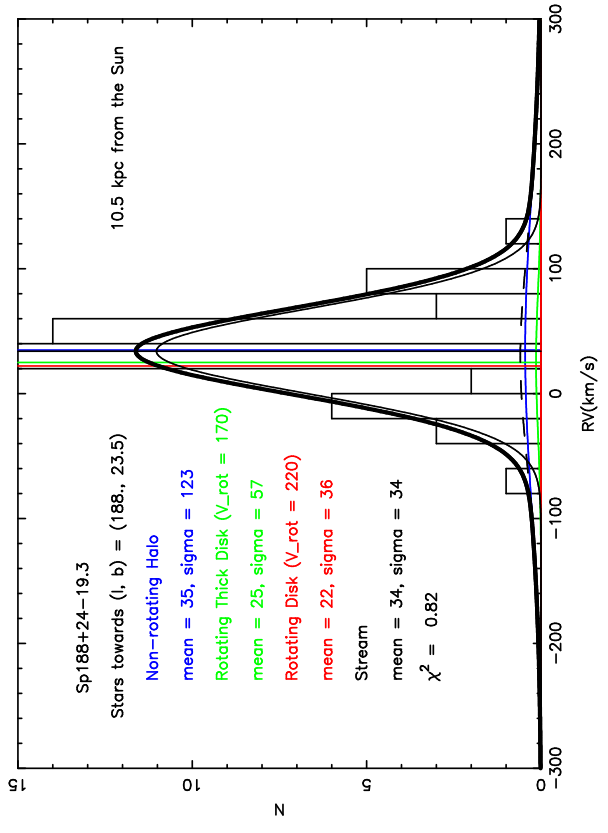
Sp188+24−19.3
Stars towards (l, b) = (188., 23.5)
10.5 kpc from the Sun
Non−rotating Halo
mean = 35, sigma = 123
Rotating Thick Disk (V_rot = 170)
mean = 25, sigma = 57
Rotating Disk (V_rot = 220)
mean = 22, sigma = 36
Stream
mean = 34, sigma = 34
χ² = 0.82
N
RV(km/s)

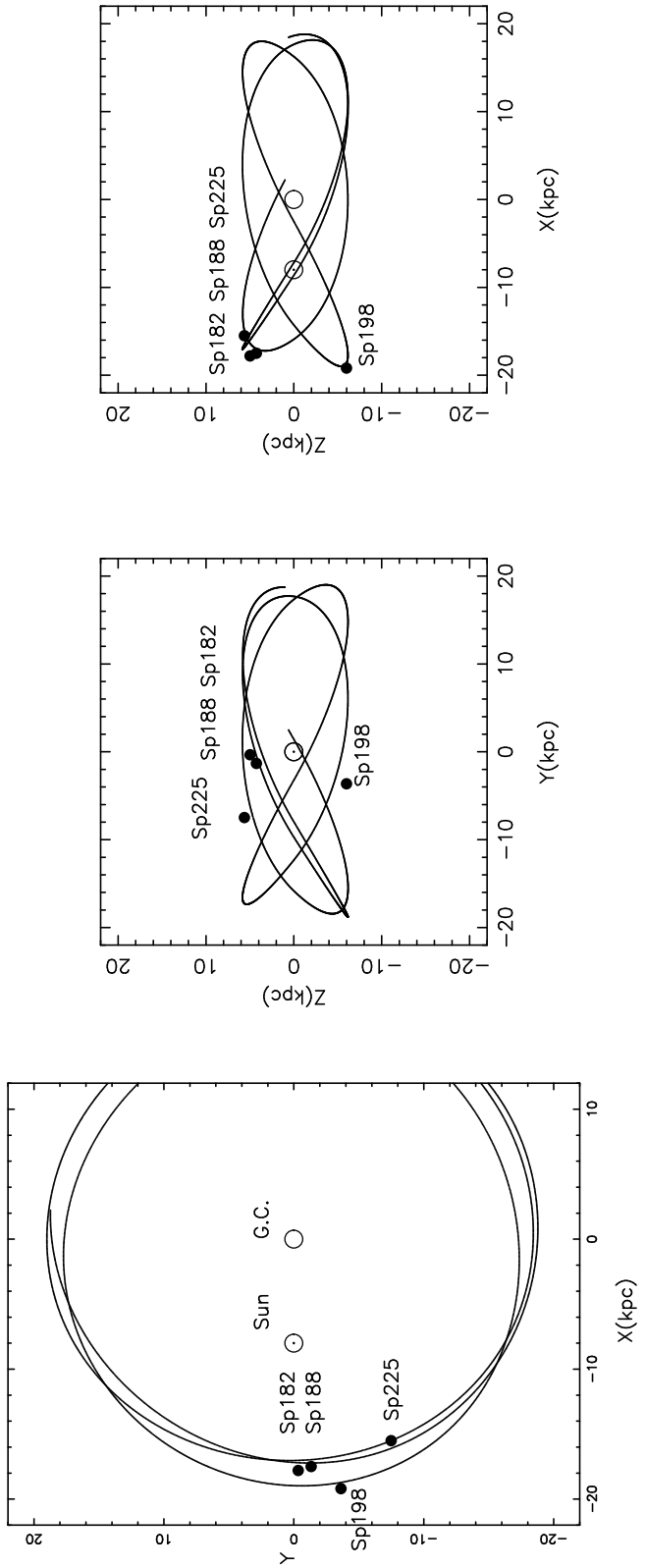
Sp182 Sp188 Sp225
Sp198
Z(kpc)
X(kpc)
Sp225 Sp188 Sp182
Sp198
Z(kpc)
Y(kpc)
G.C.
Sun
Sp182
Sp188
Sp225
Sp198
Y
X(kpc)

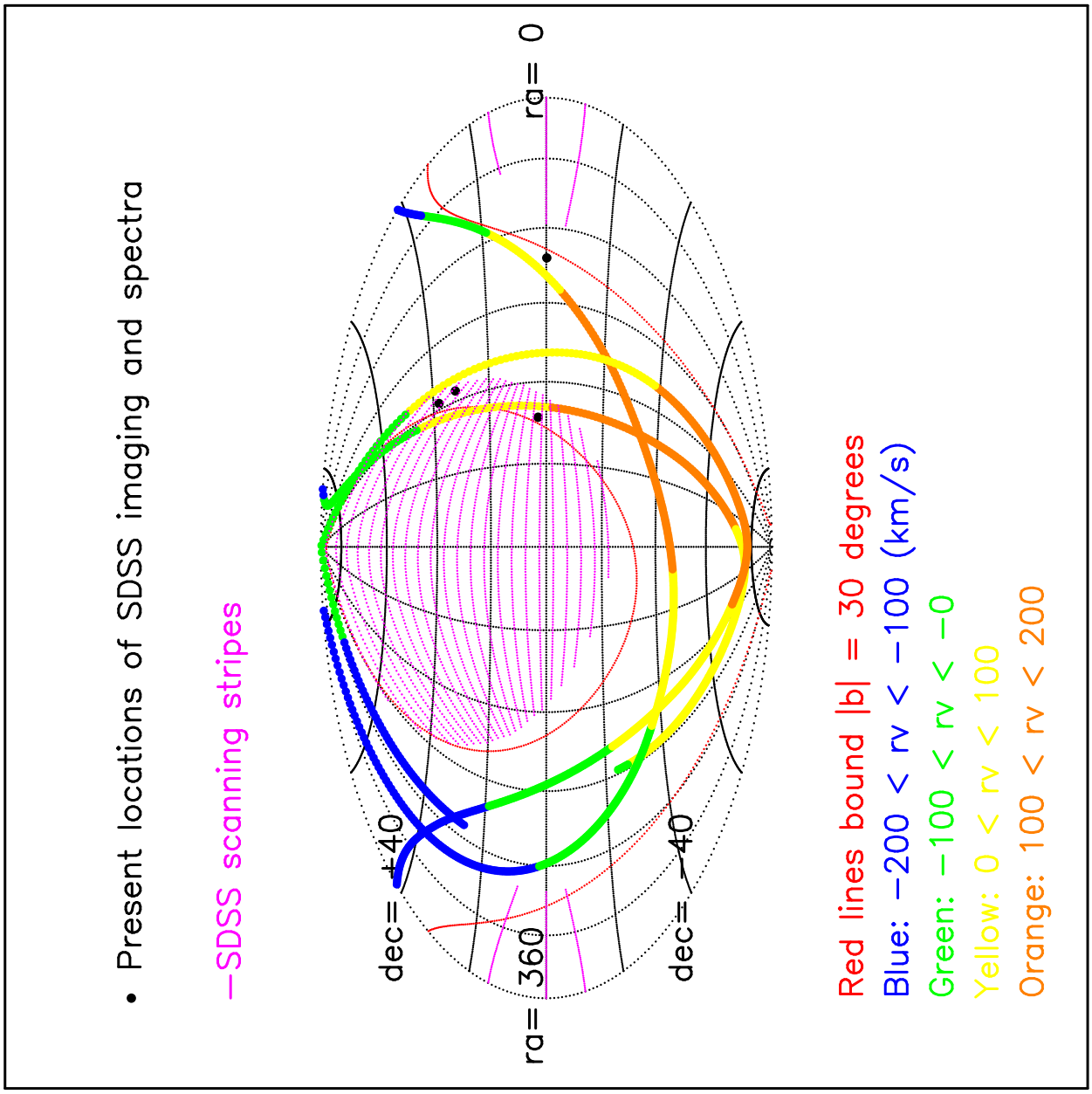
• Present locations of SDSS imaging and spectra
–SDSS scanning stripes
ra= 0
ra= 360
dec= +40
dec= −40
Red lines bound |b| = 30 degrees
Blue: −200 < rv < −100 (km/s)
Green: −100 < rv < −0
Yellow: 0 < rv < 100
Orange: 100 < rv < 200

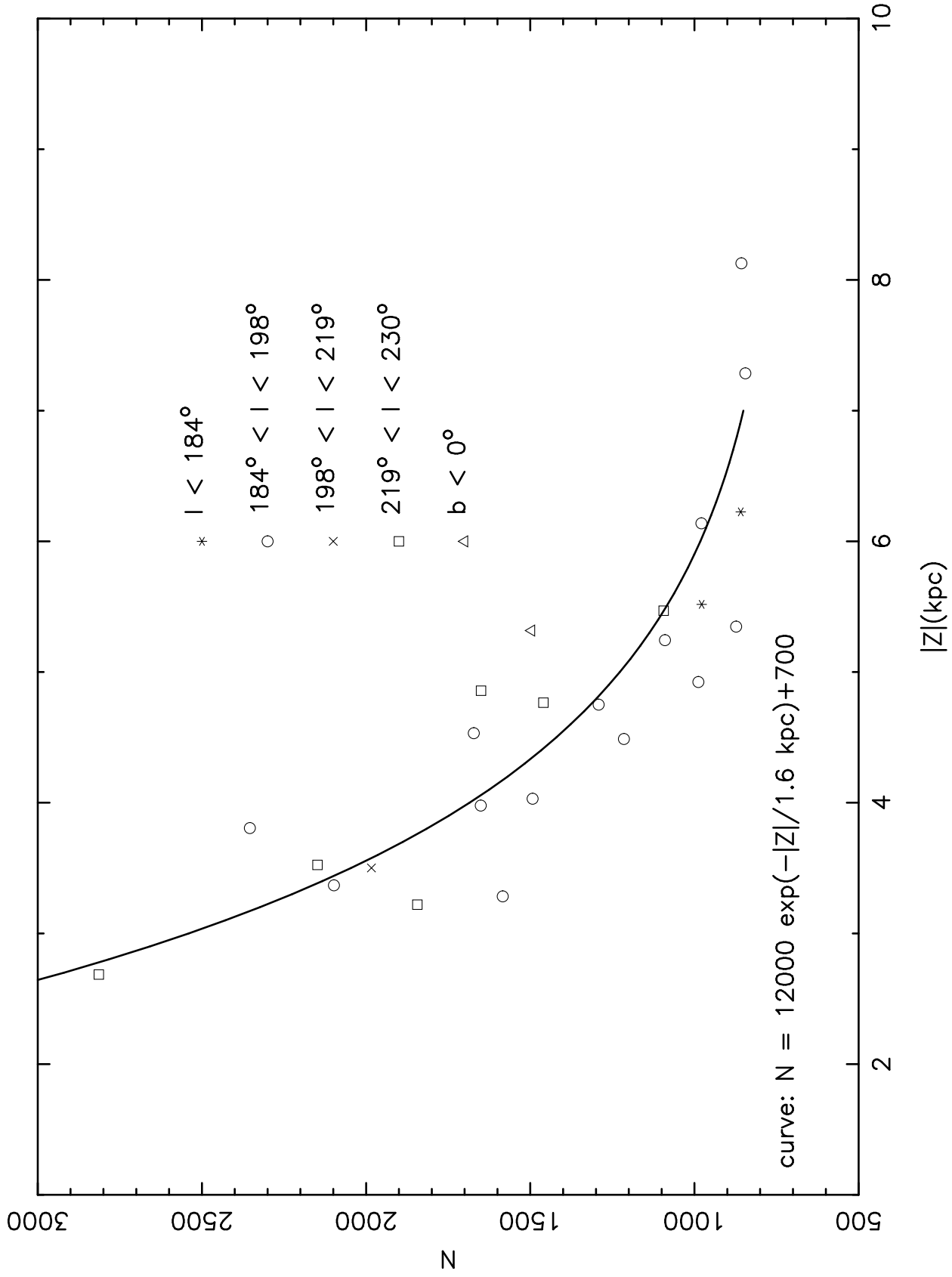
N
|Z|(kpc)
curve: N = 12000 exp(−|Z|/1.6 kpc)+700
l < 184°
184° < l < 198°
198° < l < 219°
219° < l < 230°
b < 0°
500
1000
1500
2000
2500
3000
2
4
6
8
10

1. Erratum: A Low Latitude Halo Stream around the Milky Way

The zeropoints of the stellar templates used to measure radial velocity in the main body of this paper have been found to be systematically in error. Correction of the radial velocities significantly increases the derived circular velocity of the stars in the planar stream to $215 \pm 25\,\mathrm{km\,s^{-1}}$. The velocity dispersion of the stream is somewhat lower than earlier results with the modified analysis.

Two types of stars were studied in this paper. The original template for stars of type F, used to study the "Monoceros arc" Galactic structure, was incorrectly zeropointed by -20 $\mathrm{km\,s^{-1}}$. The original template for stars of type A, used to measure the Sagittarius dwarf tidal stream, produced radial velocities systematically shifted by -49 $\mathrm{km\,s^{-1}}$.

A cross-correlation of Sloan Digital Sky Survey (SDSS) spectra with templates from the ELODIE survey (Soubiran, Katz and Cayrel 1998) was performed to find new radial velocities for each star (D. Schlegel, private communication). This showed that our radial velocities were systematically shifted by an amount that depends on the type of the star observed and on the original template against which it was cross-correlated.

To determine the measurement error with the new templates, we identified 445 F-type stars and 1109 A-type stars which had been observed twice by the SDSS. These stars were chosen with the color and magnitude criteria used to select stars in Figures 6 and 9. The errors in the F stars were a good match to a Gaussian with a sigma of 28 $\mathrm{km\,s^{-1}}$. The errors in the A star comparison were significantly non-Gaussian, with large tails. A χ^2 fit to a Gaussian (similar to the technique we use in this paper to measure the width of the streams) yielded a sigma of 35 $\mathrm{km\,s^{-1}}$. Dividing by $\sqrt{2}$ to reflect two independent measurements, we derive a random error of 20 $\mathrm{km\,s^{-1}}$ for F stars and 25 $\mathrm{km\,s^{-1}}$ for A stars. The template matching errors in these blue (type A) stars using ELODIE spectral templates are somewhat larger than the errors with our previous analysis, but we found it useful to use ELODIE spectral templates to ensure that the zeropoints were accurate.

Additionally, we examined the measured stellar stream dispersions. Electronic versions of Figure 2, Figure 6, and Figure 9 of our paper are presented here with the corrected radial velocity determinations. The data were selected as described in the original paper.

Table 1 has been regenerated in its entirety, replacing columns 8 and 10. The radial velocity in column 8 has been replaced with the radial velocity determined from cross-correlation with ELODIE templates. The status flag in column 10 now indicates stars which were used to generate Figure 2. A "0" indicates that the star was either outside of the color box or had a high cross-correlation error, and a "1" indicates that the star was used to fit stream properties.

Table 2 has been regenerated using the new results as well. Column 10 has been added to indicate the estimated number of spectra in the stream component. These numbers are used to compute the error in radial velocity, as described in the original paper. Column 11 shows the corrected circulation velocities, which are now consistent with Crane, et al. (2003). Note that the velocity dispersions of the planar stream are even tighter than originally measured, strengthening the case that the motion is coherent. Note that the mean velocity of the Sagittarius stream in the direction $(l, b) = (165°, -55°)$ is -160 km s^{-1}, in line with recent simulations by Martinez-Delgado et al. (2003).

We would like to acknowledge Steve Majewski, who initially pointed out to us that radial velocities for stars he had measured in the halo streams were different from our radial velocities by 20 to 50 km s^{-1} (Crane, et al. 2003). We also acknowledge T. Beers, C. Prieto, and R. Wilhelm for an independent RV analysis, with which we could compare our measured radial velocities.

REFERENCES

Crane, J. D., Majewski, S. R., Rocha-Pinto, H. J., Frinchaboy, P. M., Skrutskie, M. F., & Law, D. R. (2003), ApJ, 594, L119

Martinez-Delgado, D., Gomez-Flechoso, M. A., Aparicio, A., & Carrera, R., ApJ, in press, astro-ph/0308009

Soubiran, C., Katz, D., & Cayrel, R. (1998), AAS, 133, 221

Figure 2 caption (revised version): Histogram of radial velocities for 234 blue stars with $19.1 < g_0 < 20.3$ and $0.158 < (g-r)_0 < 0.3$ in the direction $(l, b) = (198°, -27°)$. Stars with radial velocity errors (as determined from cross correlation with an ELODIE template of similar spectral type) of over 20 $\mathrm{km\,s^{-1}}$ were rejected. The stars have an average heliocentric radial velocity of 54 $\mathrm{km\,s^{-1}}$ with a remarkably small 1D velocity dispersion of $\sigma = 18$ $\mathrm{km\,s^{-1}}$ after subtraction in quadrature of typical instrumental errors of 20 $\mathrm{km\,s^{-1}}$. The distance to the stars was calculated from the turnoff magnitude listed in Table 2, assuming an absolute magnitude of $M_g = 4.2$ for turnoff stars. Also plotted are several models, representing expected contributions and projected radial velocities of stars from the Milky Way's thin disk (red) and thick disk (green), both negligible, for objects of this color at this distance from the Galactic center, and for the stellar spheroidal halo (blue). The black dotted line is the sum of the thin disk, thick disk and halo components and the thin solid line represents a Gaussian fit to the 'extra' stars, where the contribution of the halo has been adjusted to minimize the overall fit (thick black line). The density excess and narrow dispersion are striking for these stars, which are apparently 20 kpc from the Galactic center.

Figure 6 caption (revised version): Histogram of radial velocities for very blue horizontal branch and blue straggler stars in the direction of the Sag South stream (Fig. 5, *black box*). As in Figure 2, stars with large radial velocity errors (as determined from cross correlation with an ELODIE template of similar spectral type) were rejected. The stars have an average heliocentric radial velocity of -160 $\mathrm{km\,s^{-1}}$ and a velocity dispersion of $\sigma \sim 22\,\mathrm{km\,s^{-1}}$, (after removing an instrumental spread of $25\,\mathrm{km\,s^{-1}}$).

Figure 9 caption (revised version): Histograms of radial velocities, with Galactic model fits, for the spectra of stars of the last four entries of Table 2. The distance to the stars was calculated from the turnoff magnitude listed in Table 2, assuming an absolute magnitude of $M_g = 4.2$ for turnoff stars. The central velocities and velocity dispersions of three low-latitude panels are consistent with one tidal stream circling the Galaxy at a distance of 18 kpc from the Galactic center. The lower right panel shows that the low latitude structure seen in the other panels is not present at Galactic latitude $b \sim -55°$ (though one can see stars from the Sagittarius tidal stream scattering into our data at a radial velocity of about -160 $\mathrm{km\,s^{-1}}$).

Table 1. Blue stars near (l,b) = (198°, −27°) (Table Stub only – revised)

R.A. °	Dec. °	SDSS ID r-re-c-f-id	Fiber ID plate-mjd-fiber	g_0 mag	$(g-r)_0$ mag	$(u-g)_0$ mag	RV km s^{-1}	W$_K$ Å	Select Flag	E(B-V) mag
70.598290	-0.213427	0125-7-3-546-0318	797-52263-318	19.632	0.232	0.984	13.1	6.19	1	0.0606
70.603553	-0.237871	0125-7-3-546-0219	797-52263-313	19.919	0.280	0.731	50.0	3.36	1	0.0573
70.622982	0.047201	0125-7-4-546-0262	797-52263-359	19.788	0.264	0.708	98.5	5.01	1	0.0768
70.625600	-0.057840	1752-0-3-332-0329	797-52263-358	19.230	0.272	1.042	66.5	4.11	1	0.0798
70.652157	-0.544781	1752-0-2-333-0301	797-52263-311	19.397	0.223	0.892	192.1	3.76	1	0.0346
70.788270	0.555787	0125-7-5-547-0374	797-52263-339	19.229	0.138	1.122	92.2	5.03	0	0.0788

Table 2. Summary of Stream detection pieces – revised

Name	α	δ	l	b	$< v_R >$	$\sigma(v_R)$	g_0[1]	$(g-r)_0$[1]	$N_{\rm stream}$	v_{circ}
Sp198-27-19.8[2]	72	0	198	-27	54 ±5	18	19.8	0.24	138	173±51
Sp225+28-19.6	133	2	225	28	78 ±6	13	19.6	0.26	33	225±29
Sp182+27-19.4	117	38	182	27	14 ±5	26	19.4	0.28	115	—
Sp188+24-19.3	115	32	188	24	19 ±5	24	19.3	0.28	75	272±120
Sag. South Strm	35	0	165	-55	-160 ±5[3]	22[3]	21.5[3]	0.22[3]	137	—

[1]mag and color of faint blue Monoceros turnoff except where indicated

[2]Plate 797

[3]For the Sagittarius stream, this $< v_R >$ and σ refer to Sagittarius stream blue horizontal branch and blue straggler stars rather than those in the Monoceros structures. The color and mag are those of the Sag. stream.

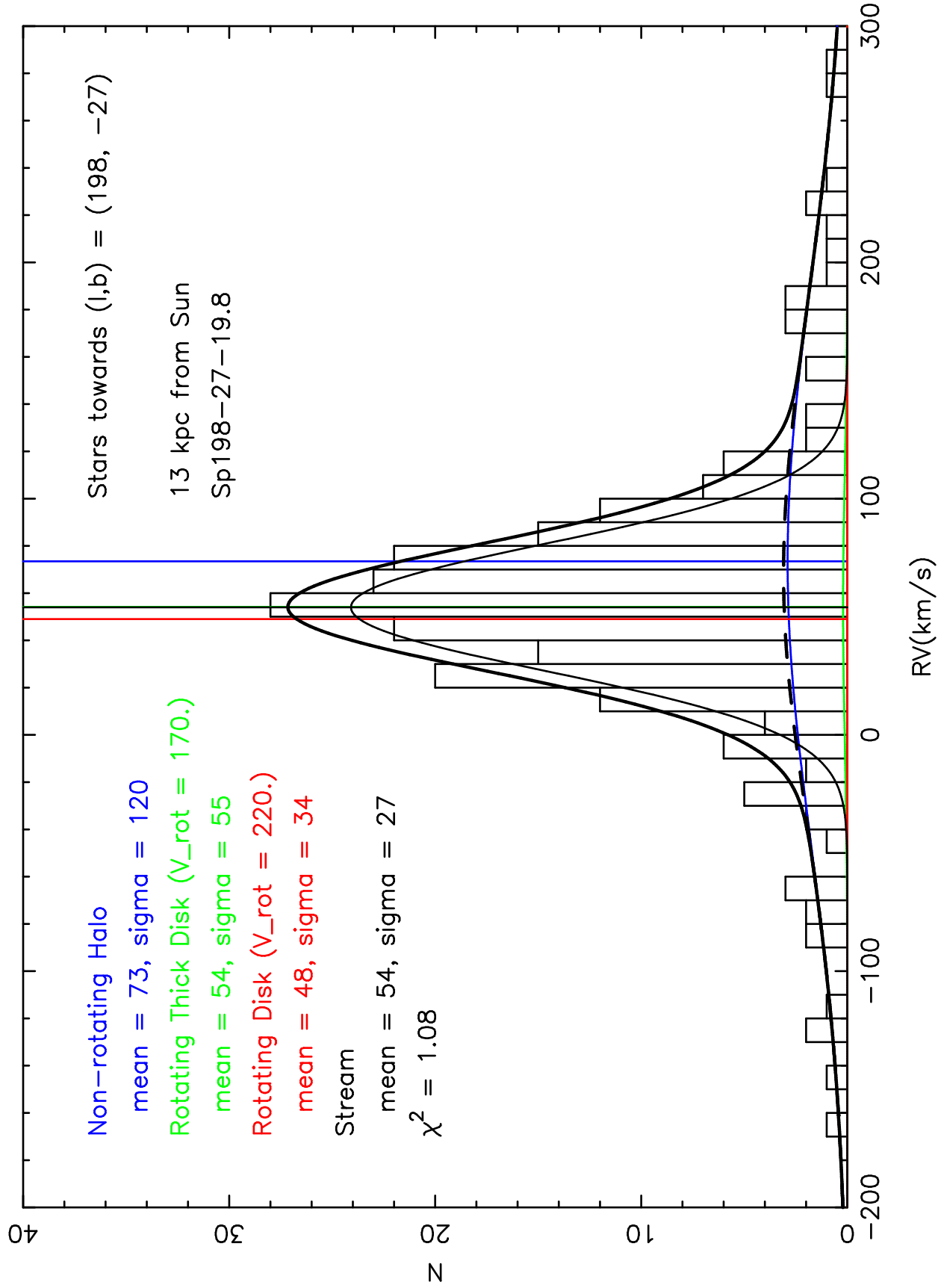
Stars towards (l,b) = (198, −27)
13 kpc from Sun
Sp198−27−19.8
Non−rotating Halo
mean = 73, sigma = 120
Rotating Thick Disk (V_rot = 170.)
mean = 54, sigma = 55
Rotating Disk (V_rot = 220.)
mean = 48, sigma = 34
Stream
mean = 54, sigma = 27
χ² = 1.08
N
RV(km/s)
0
10
20
30
40
−200
−100
0
100
200
300

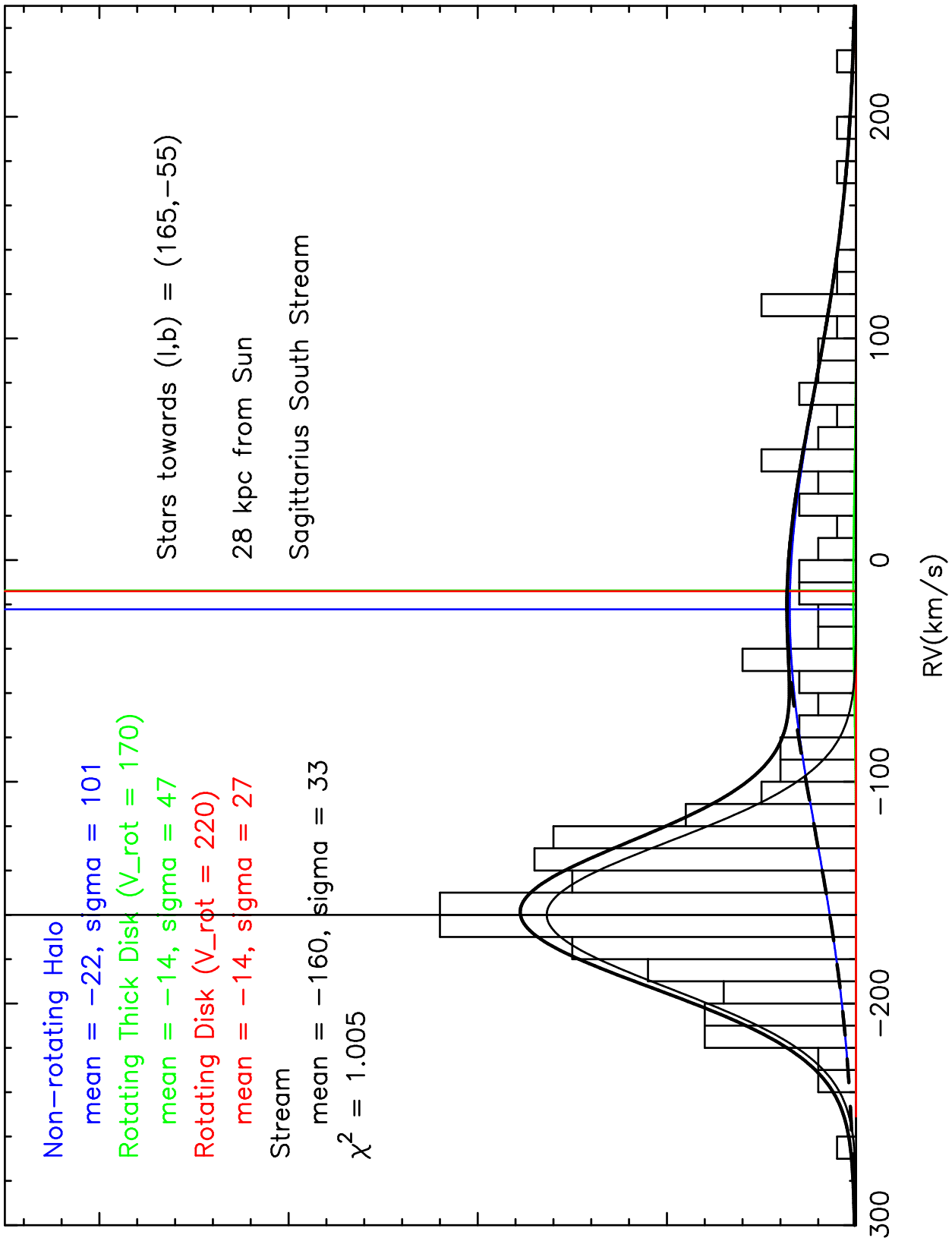
Stars towards (l,b) = (165,−55)
28 kpc from Sun
Sagittarius South Stream
Non−rotating Halo
mean = −22, sigma = 101
Rotating Thick Disk (V_rot = 170)
mean = −14, sigma = 47
Rotating Disk (V_rot = 220)
mean = −14, sigma = 27
Stream
mean = −160, sigma = 33
χ2 = 1.005
N
RV(km/s)
0
10
20
30
40
−300
−200
−100
0
100
200

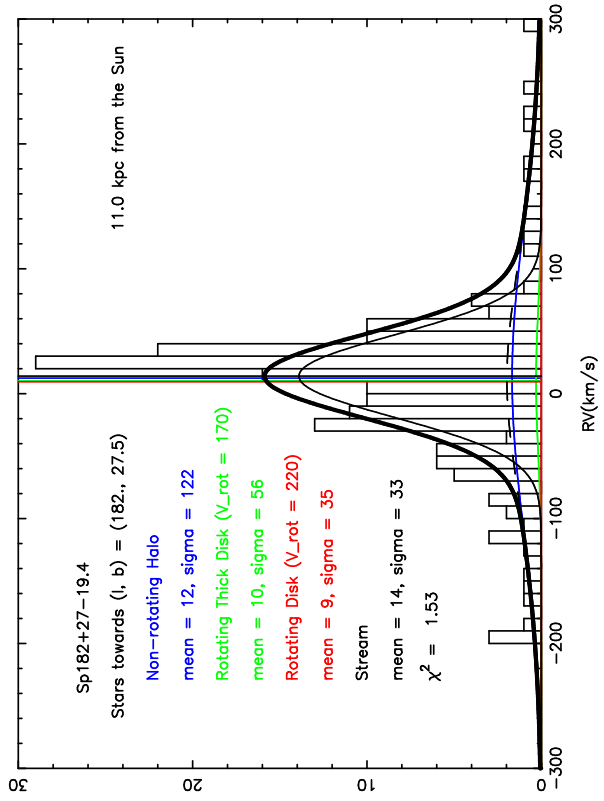
Sp182+27−19.4
Stars towards (l, b) = (182., 27.5)
11.0 kpc from the Sun
Non−rotating Halo
mean = 12, sigma = 122
Rotating Thick Disk (V_rot = 170)
mean = 10, sigma = 56
Rotating Disk (V_rot = 220)
mean = 9, sigma = 35
Stream
mean = 14, sigma = 33
χ² = 1.53
N
RV(km/s)

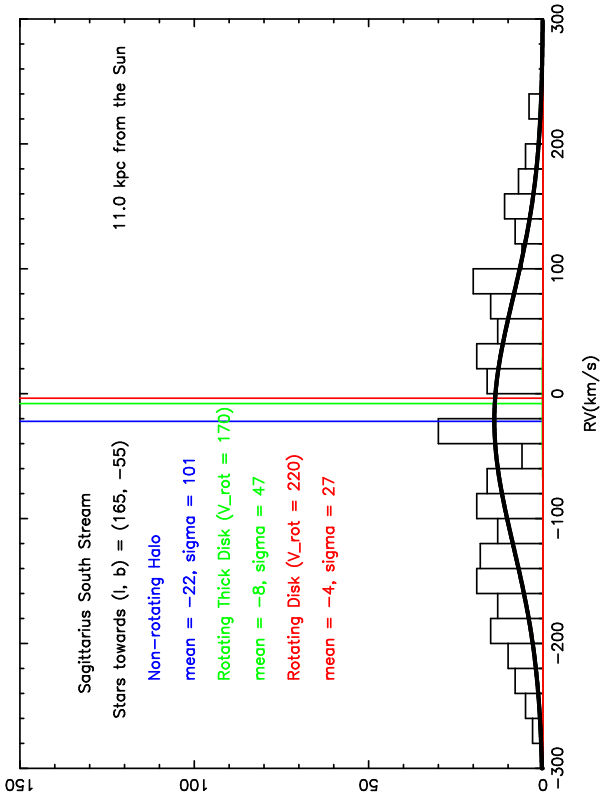
Sagittarius South Stream
Stars towards (l, b) = (165, −55)
11.0 kpc from the Sun
Non−rotating Halo
mean = −22, sigma = 101
Rotating Thick Disk (V_rot = 170)
mean = −8, sigma = 47
Rotating Disk (V_rot = 220)
mean = −4, sigma = 27
N
RV(km/s)

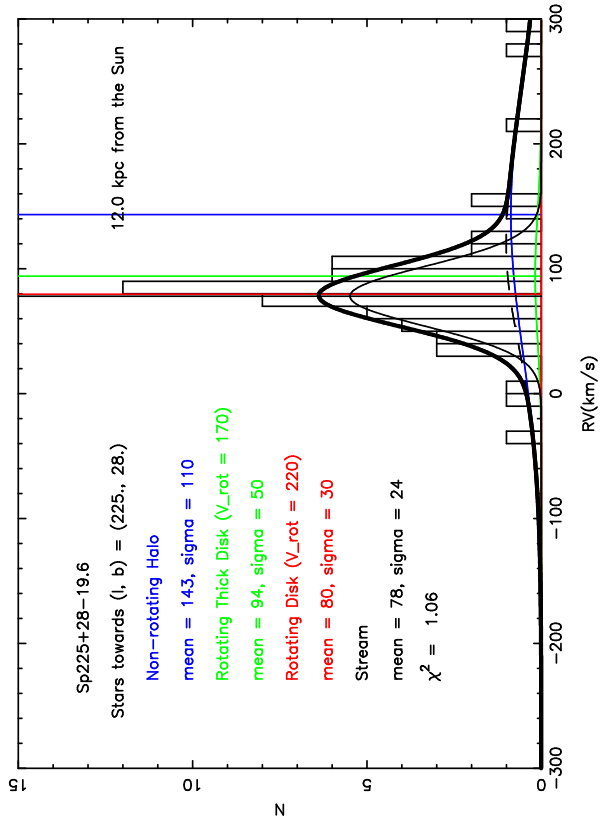
Sp225+28−19.6
Stars towards (l, b) = (225., 28.)
12.0 kpc from the Sun
Non−rotating Halo
mean = 143, sigma = 110
Rotating Thick Disk (V_rot = 170)
mean = 94, sigma = 50
Rotating Disk (V_rot = 220)
mean = 80, sigma = 30
Stream
mean = 78, sigma = 24
χ² = 1.06
N
RV(km/s)

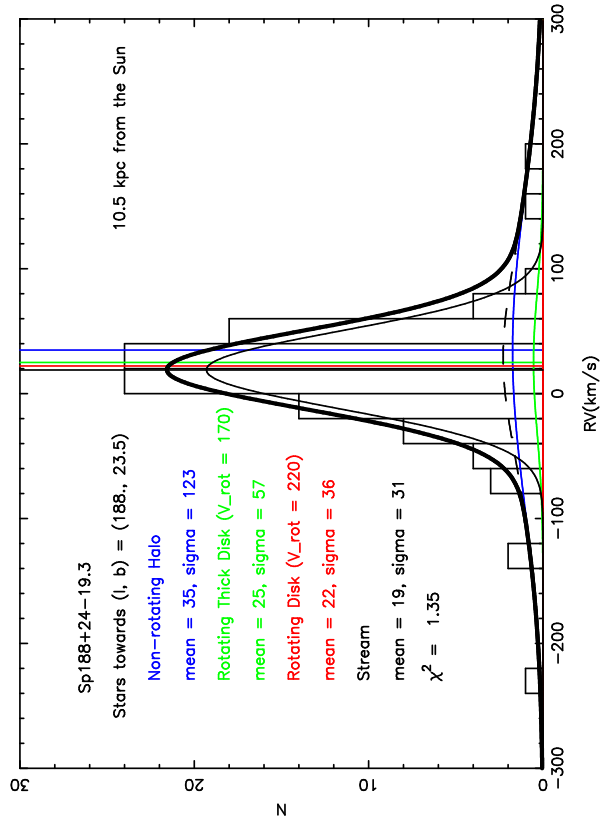
Sp188+24−19.3
Stars towards (l, b) = (188., 23.5)
10.5 kpc from the Sun
Non−rotating Halo
mean = 35, sigma = 123
Rotating Thick Disk (V_rot = 170)
mean = 25, sigma = 57
Rotating Disk (V_rot = 220)
mean = 22, sigma = 36
Stream
mean = 19, sigma = 31
χ² = 1.35
N
RV(km/s)